Sequential development of interfering metamorphic core complexes: numerical experiments and comparison with the Cyclades, Greece

C. TIREL[1,2]*, P. GAUTIER[3], D. J. J. VAN HINSBERGEN[4] & M. J. R. WORTEL[1]

[1]*Department of Earth Sciences, Faculty of Geosciences, Utrecht University, Budapestlaan 4, 3584 CD Utrecht, The Netherlands*

[2]*Current address: Dublin Institute for Advanced Studies, Geophysics Section, 5 Merrion Square, Dublin 2, Ireland*

[3]*Université Rennes 1, Géosciences Rennes UMR 6118 CNRS, Campus de Beaulieu, 35042 Rennes, France*

[4]*Paleomagnetic Laboratory 'Fort Hoofddijk', Faculty of Geosciences, Department of Earth Sciences, Utrecht University, Budapestlaan 17, 3584 CD Utrecht, The Netherlands*

**Corresponding author (e-mail: celine@cp.dias.ie)*

Abstract: The mechanics of metamorphic core complex (MCC) development and the associated process of lower crustal flow have been the topic of several modelling studies. The model setup usually includes a local heterogeneity forcing deformation to localize at a given site, enabling only one MCC to develop. This paper presents numerical lithospheric-scale experiments in which deformation is not *a priori* localized in a specific place, in order to examine whether multiple MCCs could develop during extension, at which conditions, and how. Configurations with either a single MCC or several far-distant MCCs aligned in the section parallel to extension are obtained for a relatively wide range of initial conditions, the only firm requirement being that the lower crust and the sub-Moho mantle both have very low strengths. In contrast, only a narrow range of conditions leads to the development of closely spaced MCCs. In this case, the MCCs interfere with one another (the domes are partly superimposed or/and share a shear zone in common) and develop in sequence. This configuration is compared with the Cyclades archipelago, where closely spaced chains of MCCs have been described in the literature. A review of available data on the islands documents a good agreement with the experiments in terms of final depth of the Moho, geometry and kinematic pattern of the MCCs, and timing of exhumation of the metamorphic rocks. Based on this agreement, we tentatively deduce from the numerical results some of the conditions that prevailed at the initiation of, and during, post-orogenic MCC-type extension in the Cyclades. The most likely initial thickness of the crust is between 40 and 44 km. A thermal lithospheric thickness of only *c*. 60 km is also likely, which might be a condition at the onset of extension or may have been obtained during early stages of extension while the lithosphere was warmed up. Either a backarc subduction setting or a process of mantle delamination may account for this situation. The numerical results also suggest a boundary velocity of 2.0–2.3 cm/a, which should basically reflect the rate at which the South Hellenic subduction zone retreated. Considering *c*. 500 km as an upper bound for the amount of retreat balanced by Aegean extension and assuming that this retreat mostly occurred during MCC-type extension in the Cyclades, we find that the boundary velocity could have been as high as 2.1 cm/a if MCC-type extension lasted 24 Ma, starting at *c*. 30 Ma and finishing at *c*. 6 Ma, as suggested by available geochronological data. A velocity of 2.1 cm/a agrees well with the numerical results.

Metamorphic core complexes (MCCs) are typical structures in regions made up of highly extended continental lithosphere (e.g. Coney 1980; Lister *et al.* 1984; Burg *et al.* 1994; Jolivet *et al.* 1998). They constitute metamorphic domes capped by one or several low-angle normal-sense shear zones (or 'detachment' zones) that separate a highly faulted hanging wall made up of superficial rocks from a footwall made up of rocks exhumed from the middle or lower crust and recording a progressive change from ductile to brittle behaviour (Fig. 1). As such, MCCs reflect highly localized extensional strain on the scale of the crust. As a result, the corresponding region could be expected to show pronounced lateral variations of the Moho depth. Yet, in regions where MCCs are found, the Moho commonly displays a flat geometry, like in the Basin and Range province (Hauser *et al.* 1987;

From: VAN HINSBERGEN, D. J. J., EDWARDS, M. A. & GOVERS, R. (eds) *Collision and Collapse at the Africa–Arabia–Eurasia Subduction Zone*. The Geological Society, London, Special Publications, **311**, 257–292.
DOI: 10.1144/SP311.10 0305-8719/09/$15.00

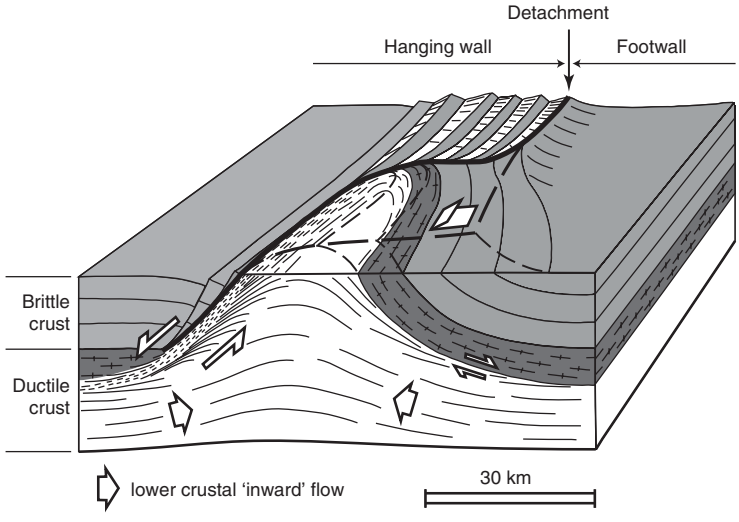

Fig. 1. Simplified sketch showing the main features of a metamorphic core complex, modified after Brun & van den Driessche (1994).

McCarthy & Thompson 1988) and in the Aegean domain (Makris 1978; Sachpazi *et al.* 1997; Tirel *et al.* 2004*b*; Endrun *et al.* 2008). Pervasive flowing of the lower crust, thought to be possible if the rocks are of sufficiently low viscosity, is usually viewed as the most likely mechanism accounting for the flatness of the Moho in such regions (e.g. Block & Royden 1990; Buck 1991; Wernicke 1992; Brun & van den Driessche 1994; McKenzie *et al.* 2000).

The mechanics of MCC development and associated process of lower crustal flow have been addressed in several analytical, numerical and analogue modelling studies so far (Block & Royden 1990; Buck 1991; Wdowinski & Axen 1992; Brun *et al.* 1994; Rosenbaum *et al.* 2005; Wijns *et al.* 2005; Tirel *et al.* 2006; Gessner *et al.* 2007). In these studies, the modelling setup is generally concerned with the crust only; the way extension is accommodated in the underlying mantle is not addressed. More recently, Tirel *et al.* (2004*a*, 2008) have carried out numerical experiments with a setup encompassing the subcrustal mantle. Among these experiments, those involving a very high initial geothermal gradient are characterized by a greater complexity in the development of detachment zones, with commonly several synthetic and antithetic shear zones being formed in sequence during the growth of a single large MCC. In other words, these experiments tend to display strain delocalization during extension. However, for the purpose of a parametric analysis, this study needed to share the same shortcoming as previous studies did: the initial setup included a local heterogeneity forcing deformation to localize at a given site, enabling only one MCC to develop.

In the present study, we have performed new lithospheric-scale experiments in which deformation is not *a priori* localized in a specific place (the initial model is perfectly homogeneous laterally, and the grid is randomly distributed), in order to examine whether multiple MCCs could develop during extension, at which conditions, and how. A relatively wide range of initial conditions produced two-dimensional numerical configurations with either a single MCC or several far-distant MCCs aligned in the section parallel to extension. Extrapolated to a three-dimensional setting, the latter case suggests that distinct subparallel chains of MCCs could be a common situation in nature, provided the appropriate conditions are maintained over a region wide enough. In contrast, only a narrow range of conditions led to the development of closely spaced MCCs. In this case, because of the close spacing, the MCCs interfere with one another (the domes are partly superimposed or/and share a shear zone in common) and develop in sequence. The fact that this configuration is obtained for only a narrow range of conditions suggests that it should be rare in nature. Conversely, if it is observed in a natural setting, some insight may be gained from the experiments about the mechanics of extension and the physical properties of the lithosphere at the onset of the extensional event in the region.

The case of several MCCs aligned in a section parallel to the direction of extension is not uncommon worldwide. Examples may be found in the North American Cordillera (Coney 1980; Wust 1986), especially in the southernmost Basin and Range (Davis 1980) and around the border between USA and Canada (Parrish *et al.* 1988; Vanderhaeghe & Teyssier 2001), also possibly at

the latitude of the Snake Range and in the central Basin and Range (Wernicke 1992). The French Massif Central provides another example (Burg *et al.* 1994; Vanderhaeghe & Teyssier 2001). In the Mediterranean area, this situation is encountered in the northern Tyrrhenian domain (Jolivet *et al.* 1998) and, within the Aegean domain, in the Cyclades archipelago (Lister *et al.* 1984; Gautier & Brun 1994*a*, *b*; Jolivet *et al.* 2004) and in the nearby Menderes Massif of western Turkey (Bozkurt 2001; Gessner *et al.* 2001).

The Cyclades archipelago constitutes a particularly interesting example because it has been argued earlier that the islands form closely spaced chains of MCCs that interfere with one another (Gautier & Brun 1994*a*, *b*). In the following, we first describe our numerical experiments, then review the structural and metamorphic evolution of the Cyclades. We subsequently compare the numerical results with the Cyclades. The comparison concerns the final depth of the Moho, the geometry of the MCCs, their kinematic pattern and the timing of exhumation of the metamorphic rocks. Finally, as the natural case and the experiments compare relatively well, we tentatively deduce from the numerical analysis the most likely range of conditions that prevailed in the Cyclades domain at the onset of, and during, Aegean extension.

Numerical modelling

Initial and boundary conditions

Two series of numerical experiments have been carried out to determine the conditions for development of MCCs and particularly sequential development of MCCs, as a function of initial crustal thickness, thermal structure and boundary velocity.

The model geometry consists of a rectangular box (500 × 150 km) composed of a continental crust, a lithospheric mantle and an asthenosphere with brittle–elasto–ductile properties (Fig. 2). The numerical grid consists of 250 × 75 quadrilateral bilinear elements (2 × 2 km). Each element is subdivided into two pairs of triangular sub-elements to avoid meshlocking (Cundall 1989). The mesh is randomly non-regular (random distribution of the nodes) and contains neither an anomaly in structure nor a seed that would force deformation to localize at a given site. The continental crust has an average composition of quartz-diorite with a density of 2800 kg m^{-3} (Table 1). The crust is divided into four colour marker layers to provide for a good visual tracing of the developing structures. The lithospheric mantle and the asthenosphere have an average composition of olivine with a density of 3300 kg m^{-3} (Table 1). Each numerical element is assigned a specific material phase which is defined by density and thermal and rheological parameters.

The initial temperature field is defined by a surface temperature fixed at 0 °C and a temperature of 1330 °C at the base of the lithosphere. The lateral thermal boundary conditions inhibit heat flow across vertical boundaries of the box (no heat exchange with the surrounding region).

Extension of the entire lithosphere is necessarily dependent on displacements applied at plate boundaries. Horizontal displacement with constant velocity is applied to the left boundary of the box (Fig. 2). The opposite boundary is fixed. Other boundary conditions of the numerical box are a free surface at the top of the box and a pliable Winkler basement at the bottom, which supposes free slip along both surfaces. The vertical normal stresses are proportional to the vertical displacement of the bottom boundary (Burov & Cloetingh 1997). Hydrostatic forces ensure local isostatic compensation.

Numerical method

The code PAR(A)OVOZ solves mechanical and thermal equilibrium equations in a large strain mode. This thermo-mechanical code based on

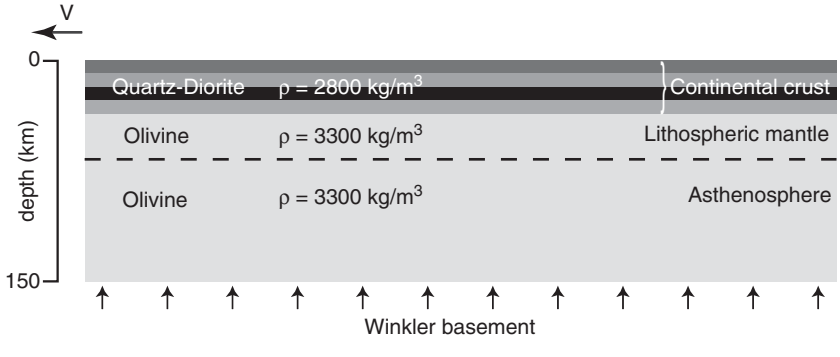

Fig. 2. Model setup used for the numerical experiments.

Table 1. *Variables and parameters used in the experiments*

Variables	Values and Units	Comments
Initial crustal thickness	30, 35, 40, 45, 50, 55, 60 km	Continental crust
Boundary velocity v	1, 1.3, 1.6, 2, 2.3, 2.6, 3 cm·yr^{-1}	Applied on left side (see Fig. 2)
Depth of the thermal lithosphere	60, 80, 100, 120 km	Applied geotherms
Parameters	**Values and Units**	**Comments**
Temperature at the base of the lithosphere	1330 °C	
Power law constant A_1	1.26×10^{-3} MPa^{-n}·s^{-1}	Quartz-diorite (crust)
Power law constant n_1	2.4	Quartz-diorite (crust)
Creep activation energy E_{a1}	219 kJ·mol^{-1}	Quartz-diorite (crust)
Power law constant A_2	7×10^{4} MPa^{-n}·s^{-1}	Olivine (mantle)
Power law constant n_2	3	Olivine (mantle)
Creep activation energy E_{a2}	520 kJ·mol^{-1}	Olivine (mantle)
Density ρ_1	2800 kg·m^{-3}	Crust
Density ρ_2	3330 kg·m^{-3}	Mantle
Thermal conductivity k_1	2.5 W·m^{-1}·K^{-1}	Crust
Thermal conductivity k_2	3.3 W·m^{-1}·K^{-1}	Mantle
Coefficient of thermal expansion	3×10^{-5} K^{-1}	
Internal heat production at surface Hs	10^{-9} W·kg^{-1}	
Specific Heat Cp	10^{3} J·kg^{-1}·K^{-1}	

FLAC® and PARAVOZ v3 (Cundall 1989; Poliakov *et al.* 1993) is a mixed finite-difference/finite element, fully explicit, time-marching Lagrangian algorithm, and has been described in several previous publications (Poliakov *et al.* 1993; Burov & Guillou-Frottier 1999, 2005; Burov & Poliakov 2001, 2003; Le Pourhiet *et al.* 2004). The description here will be limited to basic features.

The code solves the conservation equations for energy, mass and momentum:

$$\frac{\partial \rho}{\partial t} + \frac{\partial}{\partial x_i}(\rho v_i) = 0, \tag{1a}$$

where v is velocity and ρ is density, with the Newtonian equation of motion in the continuum mechanics approximation:

$$\frac{\rho \partial v_i}{\partial t} - \frac{\partial \sigma_{ij}}{\partial x_j} - \rho g_i = 0, \tag{1b}$$

$$\frac{D\sigma}{Dt} = F(\sigma, \mathbf{u}, \Delta\dot{\mathbf{u}}, \ldots T \ldots), \tag{1c}$$

where t is time, g is acceleration due to gravity, $\mathbf{u}$ is the displacement vector, T is temperature, F is the functional relationship, D is material derivative and σ is Lagrangian stress. This equation is coupled with constitutive and heat transport equations:

$$k\nabla^2 T - \rho C_p \frac{\rho T}{\partial t} + H_r = \rho C_p \mathbf{v} \cdot \nabla T \tag{2}$$

where $\mathbf{v}$ is the velocity vector, C_p is the specific heat, k is the thermal conductivity and H_r is the internal heat production per unit volume. The Boussinesq approximation is used in the equation of state to account for body forces due to thermal expansion:

$$\rho = \rho_0(1 - \alpha(T - T_0)), \tag{3}$$

where α is the coefficient of thermal expansion (Table 1). Radiogenic heating is taken into account (Table 1). The right-hand side of equation (2) is calculated directly from equation (1), whilst the left-hand side is computed using a separate numerical scheme. A dynamic relaxation technique, based on the introduction of artificial inertial masses in the dynamic system (Cundall 1989), is used to increase the internal time step and accelerate the solution of the governing equations (1).

The Lagrangian method allows the use of a small strain formulation for large strain problems because the mesh is able to move and deform with the material. At each time step, the new positions of the grid nodes are calculated from the current velocity field and updated in large strain mode accounting for the rotation of principal stress axes using Jauman's co-rotational correction:

$$\begin{cases} \omega_{ij} = \frac{1}{2}\left\{\frac{\partial \dot{u}_i}{\partial x_j} - \frac{\partial \dot{u}_j}{\partial x_i}\right\} \\ \sigma_{ij}^{corrected} = \sigma_{ij}^{small\ strain} + (\omega_{ik}\sigma_{kj} - \sigma_{ik}\omega_{kj})\Delta t \end{cases} \tag{4}$$

In quasi-static mode, the algorithm uses artificial inertial masses to suppress inertial effects and accelerate the computations (Cundall 1989). PAR(A)OVOZ also deploys a dynamic remeshing scheme,

which makes it possible to model very large displacements.

Each grid element simultaneously handles three rheological terms: brittle, elastic and ductile; thus the local deformation mode may change from dominantly brittle to dominantly ductile or elastic, depending on mechanical and temperature conditions. Material parameters for ductile creep are obtained from Hansen & Carter (1982) for quartz diorite and Goetze (1978) for olivine (Table 1).

The brittle (plastic) behaviour is described by the experimental Byerlee's law (Byerlee 1978) which is reproduced by non-associative Mohr–Coulomb plasticity with a friction angle $\phi = 30^\circ$, cohesion $C_0 = 20$ MPa and dilatation angle $\psi = 0^\circ$ (Gerbault *et al.* 1999):

$$|\tau| = C_0 - \sigma_n \tan\phi, \tag{5}$$

where τ is shear stress and σ_n is normal stress. Plastic failure occurs if the two following conditions are satisfied; shear failure criterion $f = \tau_{\mathrm{II}}^* + \sigma_1^* \sin\phi - C_0 \cos\phi = 0$ and $\partial f/\partial t = 0$ (Vermeer & de Borst 1984). In 2D formulation, $\tau_{\mathrm{II}}^* = \sqrt{(\tau_{11} - \tau_{22})^2/4 + \tau_{12}^2}$ and $\sigma_1^* = (\sigma_{11} + \sigma_{22})/2$. In terms of principal stresses, the equivalent of the yield criterion (5) is: $\sigma_1 - \sigma_3 = -\sin\phi\,(\sigma_1 + \sigma_3 - 2C_0/\tan\phi)$.

The elastic behaviour is described by the linear Hooke's law:

$$\varepsilon_{ij} = E^{-1}\sigma_{ij} - \upsilon E^{-1}\sigma_{kk}\delta_{ij}, \tag{6}$$

where repeating indexes mean summation and δ is Kronecker's operator. The values for the elastic moduli are $E = 80$ GPa (Young's modulus) and $\upsilon = 0.25$ (Poisson's ratio) (Turcotte & Schubert 2002).

The viscous (ductile) behaviour is described by an experimental uni-axial power law relationship between strain rate and stress (Kirby & Kronenberg 1987; Ranalli 1987):

$$e_{ij}^d = A(\sigma_1 - \sigma_3)^n \exp(-H/RT), \tag{7}$$

where, $H = E_a + PV$, e_{ij}^d is the shear strain rate tensor, T is the temperature in K, σ_1 and σ_3 are the principal Cauchy stresses (compression is negative), P is the pressure, V is the activation volume. A, H, E_a, and n are the material constants (Table 1) and R is the universal gas constant. The effective viscosity μ_{eff} for this law is:

$$\mu_{eff} = e_{ij}^{d(1-n)/n} A^{-1/n} \exp(H(nRT)^{-1}). \tag{8}$$

For non-uniaxial deformation, the uniaxial relationship (7) is converted to a triaxial form using the invariant of strain rate $e_{II}^d = [Inv_{II}(e_{ij})]^{1/2}$ and geometrical proportionality factors (e.g. Burov *et al.* 2003). This is needed because the rotations due to deformation can be large, and hence the invariant form of strain tensor has to be used:

$$\mu_{eff} = e_{II}^{d(1-n)/n} (A^*)^{-1/n} \exp(H(nRT)^{-1}), \tag{9}$$

where $A^* = \frac{1}{2}A_0 \cdot 3^{(n+1)/2}$.

The general constitutive viscoplastic model of the code is characterized by a visco–elasto–plastic deviatoric behavior and an elasto–plastic volumetric behaviour, with the following strain rate partitioning (M = 'Maxwell', P = 'Plastic'):

$$\dot{\varepsilon}_{ij} = \dot{\varepsilon}_{ij}^M + \dot{\varepsilon}_{ij}^P \tag{10}$$

The visco-elastic and plastic strain-rate components are thus assumed to act in series. The visco-elastic constitutive law corresponds to a Maxwell component, and the plastic constitutive law corresponds to the above-described Mohr–Coulomb model. In this implementation, the new global stress components are calculated, assuming that the principal directions have not been affected by the occurrence of plastic flow.

Numerical experiments

Exploring the conditions for MCC-type extension

To establish the initial and boundary conditions at the onset of extension, a series of experiments has been performed in order to encompass end-member situations of continental extension.

Experiments on the effects of initial crustal thickness and initial geotherms (determining the initial depth of the 1330 °C isotherm) have been carried out. Twenty-eight experiments have been performed with initial crustal thicknesses of 30 to 60 km and initial thermal lithospheric thicknesses of 60 to 120 km (Table 1). A constant horizontal displacement is applied at the left vertical boundary with v = 2.0 cm/a for each of these simulations. Figure 3a shows the initial geotherm and strength profile of the experiments with an initial crustal thickness of 30, 44 and 60 km and an initial depth of the 1330 °C isotherm at 60, 80, 100 and 120 km. The classification of three basic domains (Fig. 3b) has been made on account of the first type of structure observed in the experiments (during the first *c.* 20 Ma of extension). They are characterized by: (i) the formation of ocean floor; or (ii) the development of MCCs (considering that the main features defining a MCC are the exhumation of middle to lower crustal rocks, a detachment zone at the surface, and a flat Moho at depth); or (iii) a combination of these two processes (transitional mode). The experiments identified with

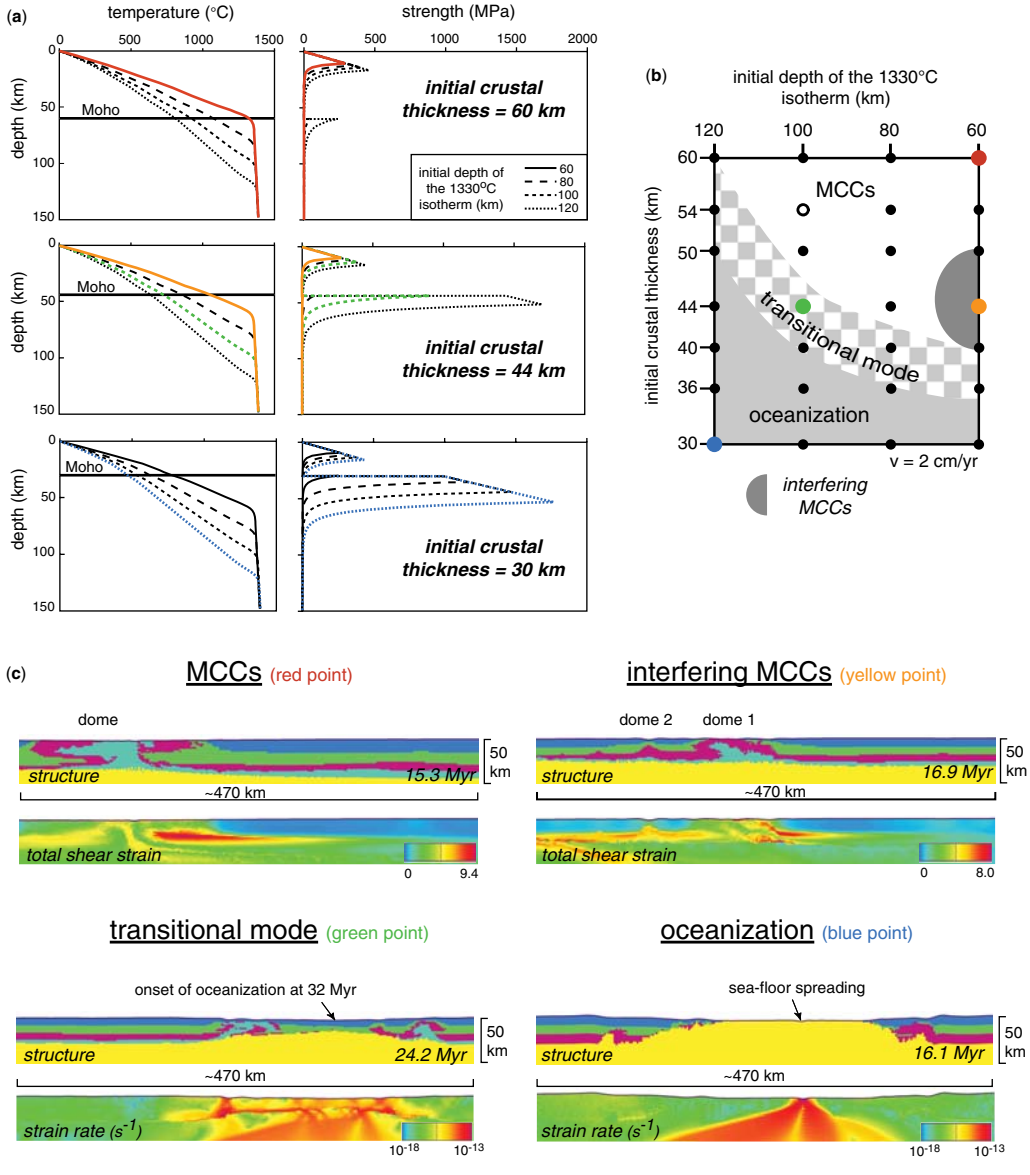

Fig. 3. Main results of the first set of numerical experiments, all performed with a boundary velocity of 2.0 cm/a. (**a**) Initial geotherm and lithosphere strength profile for a selection of experiments with an initial crustal thickness of 30, 44 and 60 km. (**b**) Distribution of the various modes of extension obtained in a series of 28 experiments (large dots) in a graph combining the initial crustal thickness with the initial depth of the thermal lithosphere (depth of the 1330 °C isotherm). (**c**) Snapshots of four experiments illustrating the different modes of extension.

colour dots in Figure 3b are shown with the same colours in Figure 3a. Figure 3c shows snapshots of these specific experiments, illustrating the general MCCs mode, the interfering MCCs mode, the transitional mode and the oceanization mode.

The oceanization mode (blue marker) is characterized by a strong necking of the entire continental crust, which results in sea-floor spreading when break-up occurs (Fig. 3c). This mode implies a high strength of the lithospheric mantle (Fig. 3a).

The MCCs domain identified in Figure 3b displays variable characteristics. Most experiments show the development of several MCCs during extension. Depending on the initial and boundary conditions, the MCCs display a large range in size and amounts of exhumation. This domain can be

subdivided into two subdomains, corresponding to two modes of extension, with either independent or interfering domes. The interfering MCCs mode (yellow marker) is obtained for a restricted set of conditions, with an initial thickness of the thermal lithosphere of *c*. 60 km and an initial crustal thickness between 40 and 50 km. A detailed description of this mode is given in the next section.

The non interfering MCCs mode is more common (Fig. 3b). An example is given in Figure 3c (red marker), which shows the development of a single huge dome. Other experiments show the development of several far-distant domes that do not interfere with one another. Such an experiment is illustrated in Figure 4 (identified with an open dot in Fig. 3b). The first timeslice (10.1 Ma) shows the exhumation of a first MCC (dome 1) and the incipient development of a graben (graben 2) which later evolves into a new MCC (dome 2 in timeslices 15.2 and 20.1 Ma). The graben is located away from the first dome (*c*. 165 km) and related shear zones (SZ1 and SZ2). While the second dome develops, new shear zones form (SZ3 and SZ4). The tips of SZ2 and SZ3 are in mutual contact but the two shear zones do not overlap, therefore SZ3 does not reactivate SZ2. Similar features are obtained for the relations between dome 2 and dome 3 and between SZ4 and SZ5 (Fig. 4). We refer to this situation as a case where the MCCs remain independent, in the sense that there is no kinematic interference between them. Nevertheless, a dynamic interference is likely, because the development of a first dome reduces the potential of lower crustal flow, thereby limiting the development of subsequent domes.

The general MCCs mode is obtained for conditions favouring the existence of a weak lower crust, with either a thick crust or a thin lithosphere (both conditions leading to high temperature conditions at the Moho) or both (Fig. 3b). In the extreme case (red marker), a huge MCC is obtained (Fig. 3c). As seen in Figure 3a, a low-strength sub-Moho mantle appears to be another necessary condition for obtaining a MCCs mode of extension with a flat Moho, as already suggested by Buck (1991). This agrees with the results obtained in a different parametric study (with a boundary velocity of 0.66 cm/a) by Tirel *et al.* (2008), who found that the development of MCCs requires an initial Moho temperature of 800 °C or higher. At these temperatures, both the sub-Moho mantle and the lower crust have low strengths and viscosities of the order of 10^{19}–10^{21} Pa.s. Figures 3a and 3b suggest that a sub-Moho mantle with a strength of only *c*. 250 MPa is enough to prevent the formation of MCCs. In addition, to obtain a MCCs mode of extension, an initial crustal thickness of at least 40 km seems required (Fig. 3b). In a thinner crust, lower crustal flow is probably hampered by the limited amount of material able to flow.

Finally, the transitional mode (green marker) is characterized by the development of MCCs of moderate size closely followed by the formation of an ocean floor (Fig. 3c), or by the formation of pseudo-MCCs showing a substantial rise of the Moho, eventually followed by the formation of an ocean.

Experiments with interfering MCCs

The conditions leading to interfering MCCs have been further investigated through a second series of experiments, in order to determine the effects of the initial crustal thickness and the boundary velocity (Table 1) on the three main properties directly comparable with geological and geophysical data;

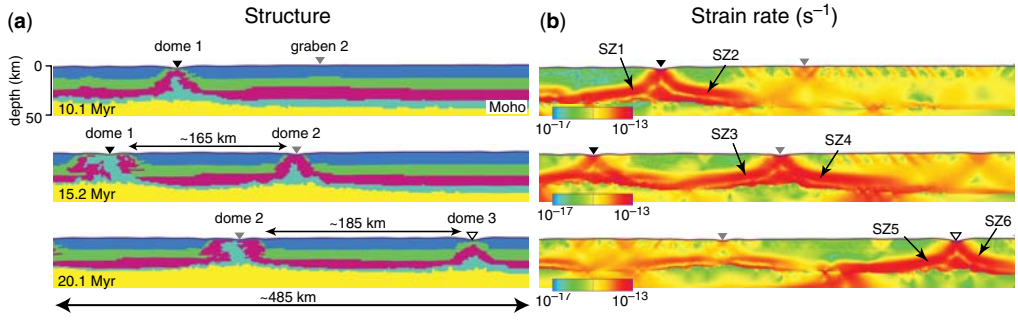

Fig. 4. Results obtained for an experiment with an initial crustal thickness of 54 km, an initial depth of the 1330 °C isotherm at 100 km, and a boundary velocity of 2.0 cm/a (cf. the open dot in Fig. 3b). This experiment illustrates the general MCCs mode of extension, in which several MCCs form but remain far-distant, so that they do not interfere. The successive timeslices are dated with respect to the onset of extension. The triangles above the surface are markers helping to locate structures from one panel to the other.

the width of the dome, the duration of dome development and the final Moho depth. The three first experiments leading to interfering MCCs have been performed with initial crustal thicknesses of 40, 44 and 50 km, an initial thermal lithospheric thickness of 60 km and a boundary velocity of 2.0 cm/a (Table 1) (Fig. 3b). In addition, six experiments have been carried out with an initial crustal thickness of 44 km, an initial thermal lithospheric thickness of 60 km and boundary velocities of 1.0, 1.33, 1.66, 2.33, 2.66 and 3.0 cm/a (Table 1). Three of these experiments show interfering MCCs. In all the experiments displaying interfering MCCs, the domes develop in sequence (one after the other). The results of the two series of experiments are shown and discussed below.

Description of two experiments. The sequential development of interfering MCCs is illustrated in Figure 5 with two experiments having an initial crustal thickness of 44 km, an initial depth of the 1330 °C isotherm of 60 km and a boundary velocity of 2.0 cm/a (Type 1 experiment, corresponding to the yellow marker in Fig. 3) or 2.33 cm/a (Type 2

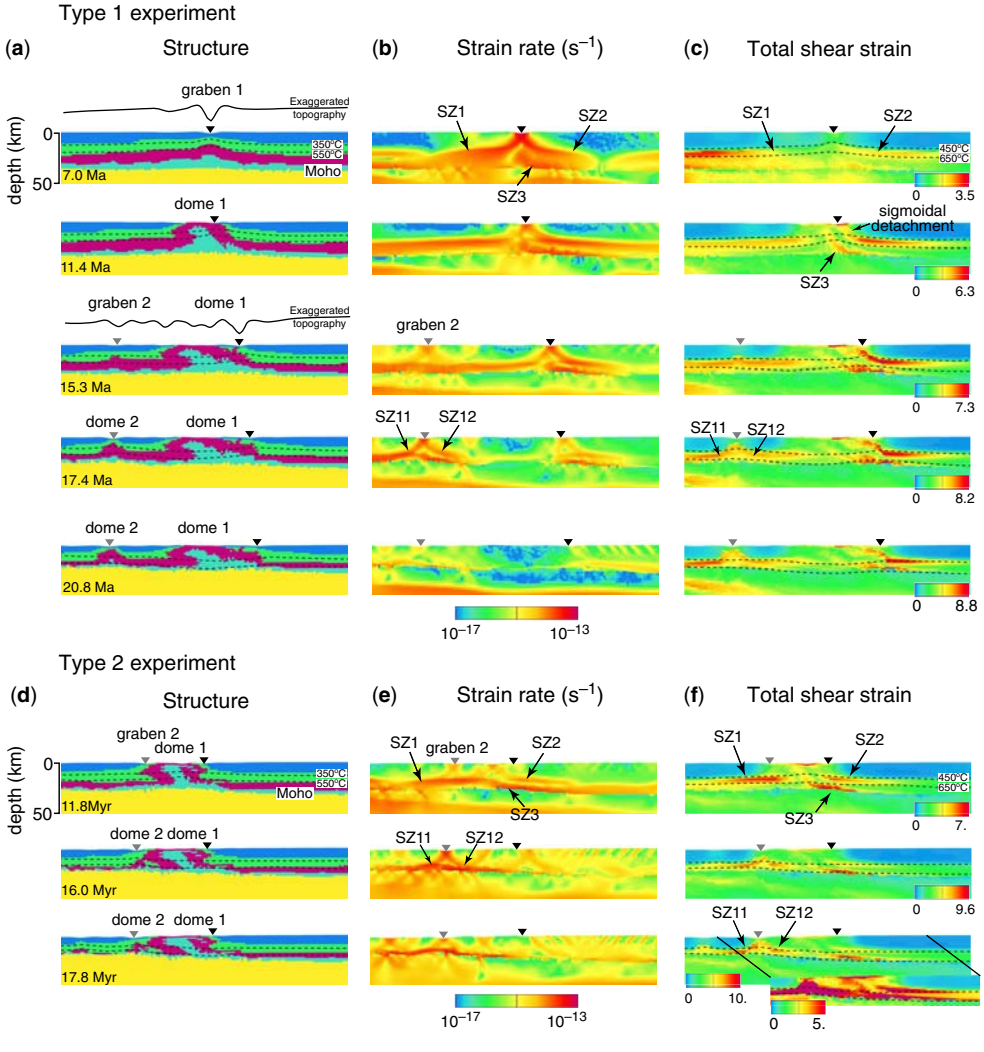

Fig. 5. Results obtained for two experiments with an initial crustal thickness of 44 km, an initial depth of the 1330 °C isotherm at 60 km, and a boundary velocity of 2.0 cm/a (Type 1, cf. the yellow dot in Fig. 3b) or 2.3 cm/a (Type 2). These experiments illustrate the interfering MCCs mode of extension. The successive timeslices are dated with respect to the onset of extension. The triangles above the surface are markers helping to locate structures from one panel to the other. A topographic profile with a vertical exaggeration of 10 is represented in (a) above the timeslices 7.0 and 15.3 Ma.

experiment). These two experiments document a similar process, differing only in terms of distance between adjacent MCCs. The model setup is shown in Figure 2. At the onset of extension, the effective viscosity of the sub-Moho mantle and the lower crust is very low (10^{19}–10^{20} Pa.s) and the two layers are coupled. The experiment of type 1 has been chosen to illustrate the entire process of exhumation. Since the process is the same, only the last stages of the second experiment are shown. The images have been truncated in order to focus on the most important crustal structures. Only a window of 280×50 km is shown. In addition to those visible in Figure 5, other domes are exhumed during each experiment, but do not interfere with one another. These independent MCCs are not shown here, nevertheless, they bear similar characteristics as those seen in Figure 4. The ages are relative to the onset of extension.

The first timeslice of Type 1 experiment, at 7.0 Ma (Fig. 5a, b, c), shows a simultaneous localization of strain in the upper and lower crust. The structure defines a symmetrical graben in the brittle crust (graben 1) and two major conjugate shear zones (SZ1 and SZ2) in the ductile middle crust (Fig. 5b, c). The two shear zones are flat-lying, located at depths around 22–25 km. A third shear zone (SZ3) develops below SZ2 at the Moho interface (Fig. 5b, c). At this stage, the ductile middle-lower crust already rises toward the surface (Fig. 5a).

The second timeslice, at 11.4 Ma, shows the development of an asymmetric dome (dome 1) following the extreme thinning of the upper crust (Fig. 5a). Middle and lower crustal levels have reached the surface and active deformation is localized mainly on the right side of the dome (Fig. 5b, c). SZ2 displays a sigmoidal shape of three parts: flat on the dome top, steeply dipping on the right dome limb and flat again in the lower crust (Fig. 5c). This forms the detachment shear zone observed at the roof of the metamorphic dome. The isotherms rise asymmetrically with respect to the dome apex (Fig. 5a), which confirms the localization of deformation along SZ2. The right side of the dome now forms the zone of lowest topography, and is a likely locus for a supradetachment basin superimposed on initial graben formation. SZ3 shows a shape similar to SZ2 but does not reach the surface. SZ3 is near-horizontal at the Moho and steeply inclined inside the dome. While still active, SZ1 has not significantly changed in shape or depth since the beginning of deformation.

At 15.3 Ma, dome 1 continues to develop with a recumbent-like fold shape (Fig. 5a). Flattening of this structure is also observed in the shape of SZ2 and SZ3 (Fig. 5c). Nevertheless, the strain rate pattern remains stable (Fig. 5b). Further left, a slight rise of the lower crust is observed (Fig. 5a), accompanied by a slight rise of SZ1 (Fig. 5c). It is related to localization of deformation in the brittle crust leading to formation of a second graben (graben 2, Fig. 5a, b). It is noteworthy that, in this experiment, graben 2 is located right above one of the previously formed shear zones (SZ1), at variance with the situation in those experiments that generated independent MCCs (Fig. 4b). In all the experiments showing a sequential development of domes, the smaller secondary dome originates from necking of the upper crust in a stage where the crustal thickness stands between 28 and 32 km and the Moho temperature is between 750 and 810 °C.

At 17.4 Ma, the shape of dome 1 has not significantly changed and the strain rate pattern indicates that active deformation has strongly decreased there, especially along SZ1 (Fig. 5a, b). A second dome (dome 2) begins to develop symmetrically, dragging SZ1 toward the surface (Fig. 5c). SZ1 is splited into two branches located on both limbs of dome 2 (SZ11 and SZ12, Fig. 5b, c). SZ12 reactivates SZ1 with an opposite, top-to-the-right sense of shear.

At 20.8 Ma, the isotherms have deepened and flattened, documenting advanced cooling of both domes (Fig. 5a). The strain rate pattern indicates an overall strong decrease in active deformation (Fig. 5b).

The initial conditions in Type 2 experiment are the same as before except for the boundary velocity, which is slightly higher. Only the three last stages are shown here (Fig. 5d, e, f). The second dome is smaller and develops closer to the first dome than in the previous experiment. As a result, there is no lid of upper crust left between the two domes. Otherwise the two experiments show similar characteristics. In both cases, the Moho remains sub-horizontal throughout the extensional process and reaches the depth of *c*. 25 km when the exhumation of MCCs has ended.

Analysis of the two experiments. Figure 6 depicts schematically the sequential development of interfering MCCs, based on the results shown in Figure 5. As previously discussed by, for example Tirel *et al.* (2004*a*, 2008), the development of MCCs may be characterized by two main stages: (1) upper crustal necking (graben formation) accompanied by the formation of flat-lying conjugate shear zones in the lower crust (Fig. 6a); followed by (2) exhumation of the dome (amplification and widening) owing to the connection, at mid-crustal depths, of the faulted graben with one of the lower crustal shear zones, forming the main detachment zone (Fig. 6b).

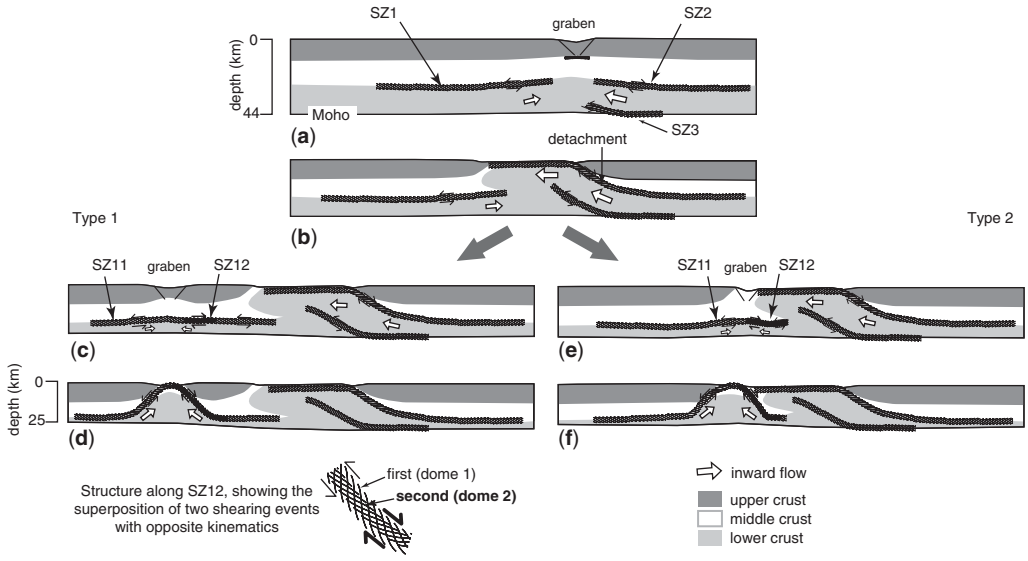

Fig. 6. Sketch based on the results shown in Figure 5, depicting the process of sequential development of interfering MCCs.

Upper crustal necking results in a reduction of the vertical lithostatic load, which induces a horizontal pressure gradient. Due to this gradient, the most ductile material at depth flows horizontally toward the area of necking. We use the term inward flow to describe this feature (cf. Brun & van den Driessche 1994). Inward flow is commonly described in MCC models as a process responsible for a flat Moho geometry (Block & Royden 1990; Wdowinski & Axen 1992; Wernicke 1992; Brun & van den Driessche 1994; Tirel *et al.* 2004*a*, 2008; Gessner *et al.* 2007). In our experiments, horizontal flow of the lower crust occurs over distances several times larger than the width of the dome and is responsible for the development of horizontal shear zones. Two convergent channel flows are systematically obtained, resulting in two conjugate flat-lying shear zones (SZ1 and SZ2; Figs 5 & 6). High strain intensities are also found within SZ3, which follows the Moho but bends upward beneath the dome apex. This particular shape is associated with fast and relatively focused rise of lower crustal material during dome amplification.

Still in the experiments, shearing due to inward flow occurs at the interface between a lower part of the crust where rocks are weak enough to flow pervasively, and an upper part where rocks are too strong to undergo significant deformation (while SZ3, at greater depth, is a mirror effect along the Moho boundary). This interface has a certain thickness, corresponding to the domain where rocks can undergo ductile shearing, in between the isotherms 450 and *c.* 650 °C (Fig. 5c). This thickness depends also partly on the resolution of the experiments. As seen in Figure 3a, we obtain a temperature of the transition between ductile and brittle behaviours of *c.* 300 °C for quartz diorite, which is the rock type we have chosen to represent the crust as a whole (note that, in our experiments, this temperature is not imposed but arises from the combination of the brittle and ductile rheological laws). Thus, in the simulations, shearing due to inward flow occurs at significantly greater depths than the ductile-brittle transition (that is, at temperatures at least *c.* 150 °C higher, corresponding to a difference in depth of about 6 km in the case of Type 1 experiment, cf. the yellow marker of Fig. 3). On the one hand, this difference is consistent with the shape of the strength profiles shown in Figure 3a, in which the brittle–ductile transition coincides with a peak in strength. In this case, shearing along the roof of a lower crustal channel may be expected to occur more readily significantly below the brittle–ductile transition. This agrees with the observation that, in Figure 3a, the temperature of 450 °C coincides with the point of inflexion along the ductile segment of the strength profile, hence marking a relatively abrupt transition between the strong ductile crust, above, and the weak one, below. On the other hand, several authors have argued that rocks immediately beneath the ductile–brittle transition may represent a low in the strength profile of the crust after a certain amount of strain is accumulated, so that this level could be used as a décollement (e.g. Handy

1989; Gueydan *et al.* 2004). If so, then it is conceivable that the roof of the shear zone overlying the lower crustal channel may coincide with the ductile–brittle transition, a situation that our experiments cannot feature. It is also worth stating that our model setup considers the crust as homogeneous; a compositionally layered crust may result in a distinct picture, with a different depth distribution of the shear zones.

In all experiments with interfering MCCs, the second MCC follows the same two-stage development as described above. Figures 6c and 6d and Figures 6e and 6f depict the results obtained in the Type 1 and Type 2 experiments, respectively, the main difference being the distance between the two domes. In both cases, localization of the second graben occurs right above SZ1 which formed during the development of the first dome. This preexisting structure is dragged toward the surface during the amplification stage of the second dome. In addition, renewed inward flow leads SZ1 to be reactivated with a similar sense of shear on the left dome limb (SZ11) but with an opposite sense of shear on the right dome limb (SZ12). This, in turn, hampers inward flow and temperature advection toward dome 1, favouring its cooling and increase in strength (cf. Fig. 5a, b). Widening of the second dome is limited because of the strong crustal thinning already achieved. Since the second dome remains small, shearing along SZ12 probably involves less strain than earlier, kinematically opposite shearing along SZ1 involves (see also Fig. 5b). Hence, relics of the first event should be found along the shear zone. In the end, the strength of the crust is too high to enable lower crustal flow any longer. If extension is to continue due to unchanged boundary conditions, it must proceed without MCCs being further developed. Until that stage, the Moho remains almost flat throughout the exhumation process. This is due to coherent ductile deformation between the lower crust and the sub-Moho mantle (see also Tirel *et al.* 2008).

Role of the initial crustal thickness and the boundary velocity. Figure 7 synthesizes the effects of modifying the initial crustal thickness or the boundary velocity on three measurable aspects of each experiment. The results shown are only for the experiments that yield interfering MCCs. The output parameters are the width of the domes (measured at the surface), the time needed to exhume the first dome (and, combining the domes, the duration of MCC-type extension), and the final depth of the Moho.

The width of the first dome (between 24 and 110 km) and the duration of its exhumation (between 11 and 24 Ma) increase with increasing initial crustal thickness and decreasing boundary velocity (Fig. 7a, b, c, d). Note that the huge dome obtained for an experiment with a 60 km-thick crust (Fig. 3b, c) is consistent with this trend.

The width of the second dome (between 15 and 30 km) and the duration of its exhumation (between 5 and 8 Ma) are much less variable than they are for the first dome. As quoted in the 'Description of two experiments' section, in all experiments, the second dome originates from necking of the upper crust in a stage where the crustal thickness lies in a narrow range, between 28 and 32 km. Hence, the width and timing of exhumation of the second dome are not directly related to the initial conditions of the experiment but to those once the first dome has essentially formed. This is consistent with the view that widening of the second dome, which depends on the possibility of renewed inward flow, is limited by the amount of crustal thinning already achieved during the development of the first dome, which itself is a function of the initial crustal thickness. In other words, the ability of the first dome to absorb a large volume of weak lower crust is proportional to the volume initially available, so that the amount of weak material left for the second dome is always nearly the same.

Combining the timing of exhumation of both domes, a duration of MCC-type extension is obtained, ranging between 16 and 32 Ma (Fig. 7c, d). The width of the whole complex made up of two adjacent domes is not plotted here. This width is related to the width of the domes but also to the distance between them. This distance is variable (cf. the difference between Type 1 and Type 2 experiments) but does not show a clear correlation with the initial crustal thickness or the boundary velocity.

After exhumation of the two domes, the Moho interface is always nearly flat. The final Moho depth (between 22.5 and 29 km) increases with increasing initial crustal thickness and with decreasing boundary velocity (Fig. 7e, f).

Geology of the Cyclades

The above two-dimensional numerical experiments suggest that, for certain conditions, MCCs may develop in sequence during continental lithospheric extension. Extrapolated to a three-dimensional setting, the corresponding region could be characterized by the development of several chains of MCC, each chain trending orthogonal or at a high angle to the direction of extension. Although such a situation may be encountered in several regions worldwide (see Introduction), we will here focus on the Cyclades archipelago because, in our view, this is the area where the existence of subparallel chains of MCC has been best documented so far. In this section, we review the structural and

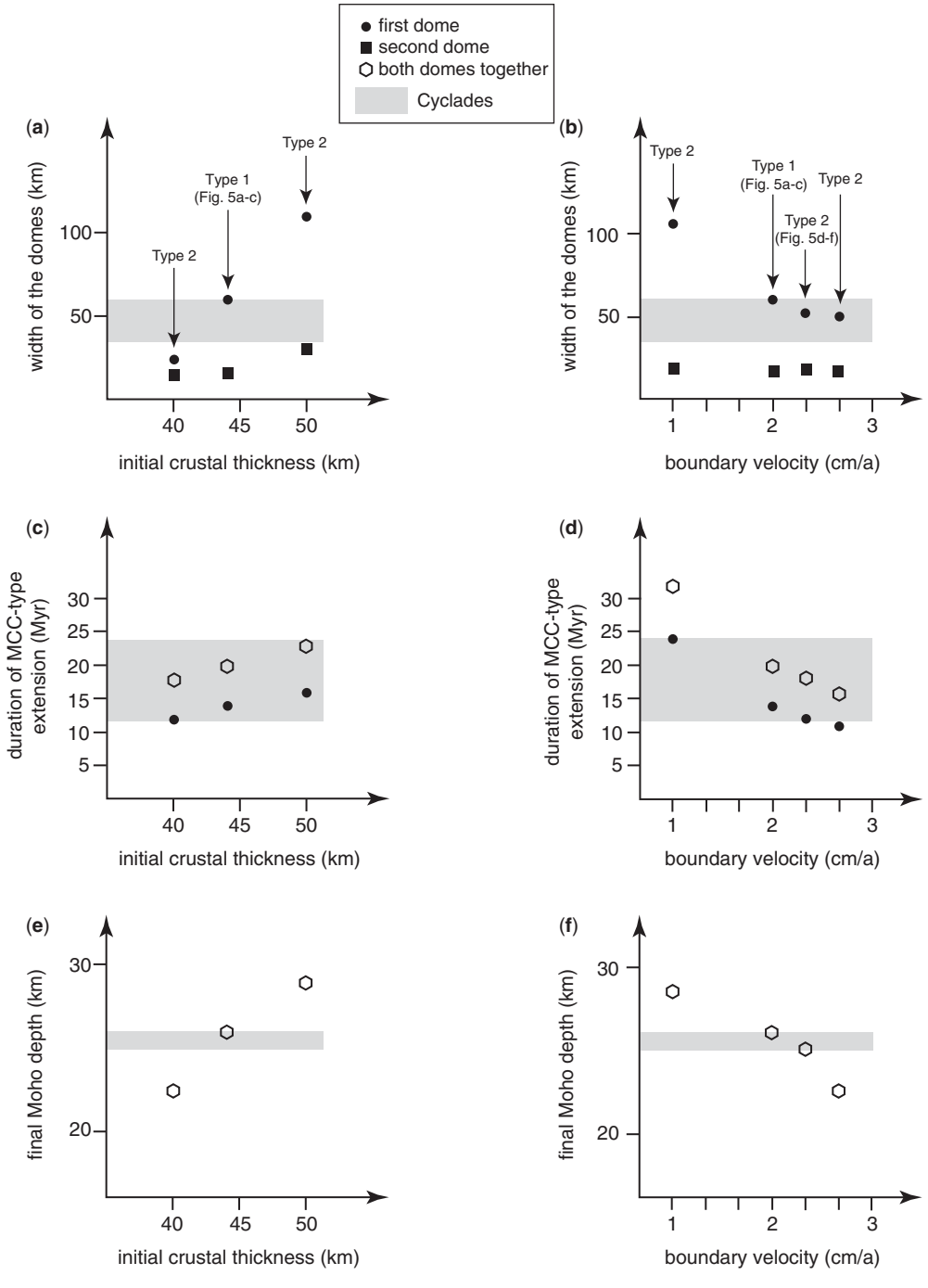

Fig. 7. Series of graphs summarizing the effects of modifying the initial crustal thickness (left) or the boundary velocity (right) on the width of the domes (top graphs), the time needed to exhume the first dome (black dot) and, combining the domes, the duration of MCC-type extension (open symbol) (middle graphs), and the final depth of the Moho (bottom graphs). Grey bands represent the range of values in the Cyclades, as deduded from available geological and geophysical data (see the text). More precisely, the grey band in (**a**) and (**b**) represents the width range for Naxos and Paros first-generation MCCs, to be compared with the numerical results obtained for the first dome only; the grey band in

metamorphic evolution of the Cyclades (see also Fig. 8), focusing on features that allow comparison with our numerical results.

Since the seminal paper of Lister *et al.* (1984), many studies have focused on the identification of extensional detachments and metamorphic core complexes in the Cyclades (e.g. Urai *et al.* 1990; Buick 1991; Gautier *et al.* 1993; Gautier & Brun 1994*a*; Vandenberg & Lister 1996; Forster & Lister 1999; Jolivet & Patriat 1999; Kumerics *et al.* 2005; Iglseder *et al.* 2006; Müller *et al.* 2006). During extension, rocks that previously recrystallized in high-pressure/low-temperature conditions were exhumed from the conditions of a greenschist facies or higher grade overprint to the conditions of brittle deformation. Granitoid intrusions were also emplaced during extension (e.g. Altherr *et al.* 1982). Time constraints indicate that these structures are broadly Miocene in age, most authors agreeing on the view that they formed during Aegean 'backarc' (or post-orogenic/post-thickening) extension. Lister *et al.* (1984) initially proposed that extension was controlled by a single south-dipping detachment zone on the scale of the Cyclades archipelago, however subsequent studies have documented a more complex structural pattern.

The Cyclades as a coherent domain during Miocene extension

Because the orientation of extension-related stretching lineations and subsequent normal faults shows a fairly abrupt change across the archipelago, it is tempting to subdivide the Cyclades into two domains. The direction of maximum stretching is NE–SW to ENE–WSW in the northwestern islands, and north–south in the southeastern islands (Gautier & Brun 1994*a*) as well as on Ikaria (Kumerics *et al.* 2005). The boundary between these two domains coincides with a NE–SW-trending fault zone extending from west of Ikaria to east of Sifnos, with probably a significant wrench (dextral) component of movement along it (Gautier & Brun 1994*a*; Gautier 1995). This fault zone has been named the Mid-Cycladic Lineament (MCL) by Walcott & White (1998). Opposite rotations across the fault zone, as documented by palaeomagnetic data on middle Miocene intrusions on Naxos, Mykonos and Tinos (Morris & Anderson 1996; Avigad *et al.* 1998), confirm the importance of the MCL and are consistent with the view that the divergent pattern of lineations seen on the scale of the Cyclades relates originally to a uniform NNE–SSW direction of stretching (Gautier & Brun 1994*b*; Walcott & White 1998; Gautier *et al.* 1999; Jolivet *et al.* 2004). This view is also consistent with the pattern of rotations on the scale of the whole Aegean region (van Hinsbergen *et al.* 2005*b*). Gautier & Brun (1994*b*) suggested that a rectilinear horst-and-graben system initially occupied the Central Aegean region and underwent progressive bending due to radial spreading of the Aegean lithosphere. Analogue experiments further showed that the presence of a thin layer of sand (simulating the brittle behaviour of the upper crust) at the top of a spreading sheet is a condition sufficient to produce a pattern of oppositely rotated blocks separated by a sharp boundary equivalent to the MCL (Gautier *et al.* 1999). Therefore, the MCL can be seen as a structure accommodating lateral variations in the rotation field of the Central Aegean region during regional extension. In contrast, Pe-Piper & Piper (2006) recently proposed a series of palinspastic reconstructions of the Aegean domain in which they assume *c*. 100 km of sinistral displacement along the MCL during the Miocene (from 17 to 5 Ma, mostly). This would imply that the Central Aegean region actually consists of two domains that were far distant from each other during early stages of core complex-type extension (Pe-Piper & Piper 2006, Figs 2 & 13). However, on account of the similarity of lithologies, tectonometamorphic evolution, and timing of exhumation of rocks on both sides of the MCL, our opinion is that the total offset across the MCL must be minor, in agreement with Walcott & White (1998).

How many MCC and detachment systems in the Cyclades?

A number of observations imply that several MCCs coexist in the Cyclades. Most islands have the geometry of a metamorphic dome defined by the orientation of foliations, occasionally also by lithological contours, and more rarely by a concentric pattern of isograds (Naxos and Paros). On several islands, a

Fig. 7. (*Continued*) (**c**) and (**d**) represents the duration of MCC-type extension in the Cyclades. The time laps for exhuming the first dome and the duration of MCC-type extension are given with respect to the onset of post-orogenic extension. Somehow arbitrarily, the time at which the first dome finishes its exhumation is taken as the time at which the second dome starts to form. Figure 5a–b shows that their developments may slightly overlap in time (i.e. shearing is still active along the frontal detachment of the first dome while the second dome rises) but also that far much of the exhumation of the first dome has occurred before the second dome forms. The time difference between the black dot and the open symbol represents the time laps for exhuming the second dome. It shows little variation, between 5 and 8 Ma.

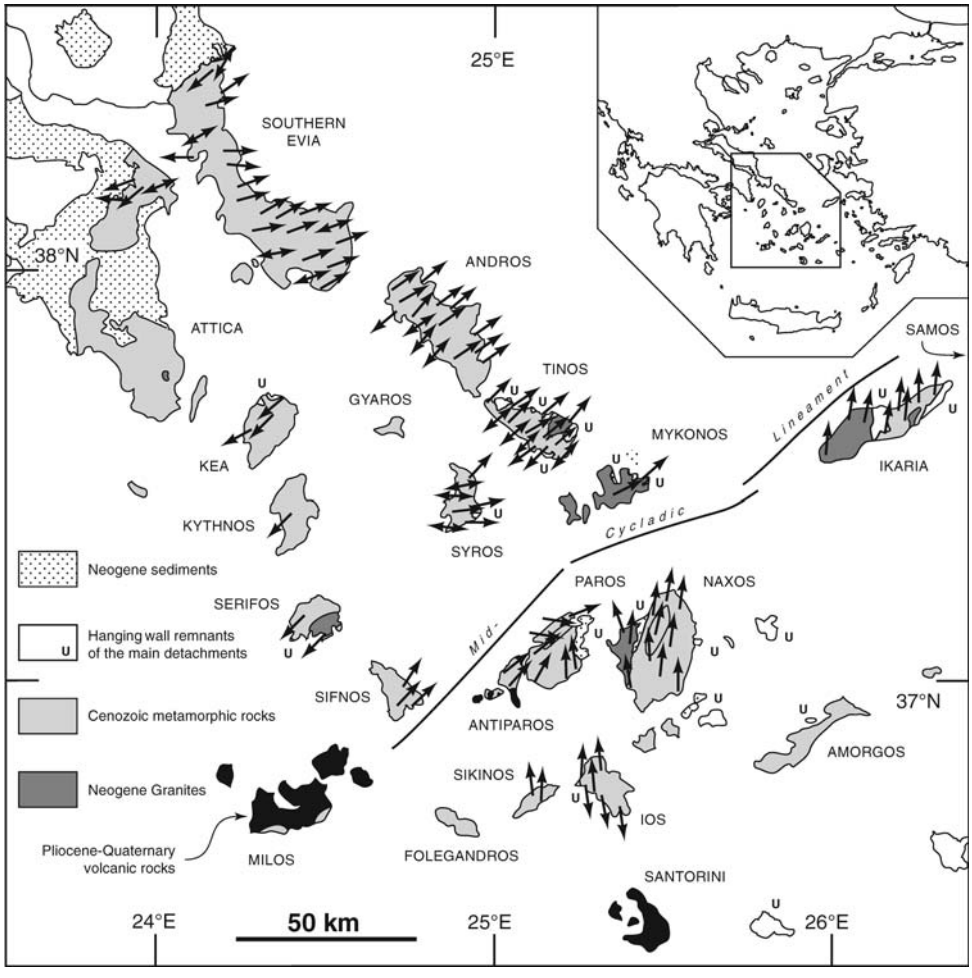

Fig. 8. Simplified geological map of the Cyclades archipelago. Arrows indicate the kinematics of extensional shearing during greenschist facies and locally higher temperature metamorphism, subsequent cooling to the conditions of brittle deformation, and within syn-kinematic intrusions. Data after Buick (1991), Gautier *et al.* (1993), Gautier & Brun (1994*a*, *b*), Gautier (1995), Vandenberg & Lister (1996), Walcott & White (1998), Jolivet & Patriat (1999), Trotet *et al.* (2001*a*), Kumerics *et al.* (2005), Iglseder *et al.* (2006) and Grasemann *et al.* (2007).

composite unit made of rocks that experienced no or limited metamorphism during the Cenozoic, rests upon the flanks of the metamorphic dome. The contact between this unit and the underlying metamorphic rocks usually bears the characteristics of an extensional detachment zone having accommodated the exhumation of the footwall rocks starting from the depths of greenschist facies and locally higher temperature metamorphism (e.g. Lister *et al.* 1984; Urai *et al.* 1990; Gautier *et al.* 1993; Gautier & Brun 1994*a*; Jolivet & Patriat 1999; Jolivet *et al.* 2004; Mehl *et al.* 2005; Müller *et al.* 2006; Grasemann *et al.* 2007). Therefore, each metamorphic dome may be described as a MCC. However, the Cyclades have also experienced Messinian–Quaternary high-angle faulting, with normal faults usually dipping away from the islands (e.g. Angelier 1977*a*, *b*; Gautier & Brun 1994*a*), so that it may be asked whether drag folding along these late faults could alone have produced the dome shape of some of the islands. This is unlikely at least on Naxos, Paros and Ios, where the domes are pronounced and regular (e.g. van der Maar & Jansen 1983; Gautier *et al.* 1993).

Occasionally, low-angle normal faults also dissect the islands and make the identification of a metamorphic dome more difficult, like on Syros (Ridley 1984).

A critical question is whether distinct MCCs found along a section parallel to extension were initially associated with a single detachment zone, as Lister *et al.* (1984) suggested, or formed beneath distinct detachment zones (Gautier & Brun 1994*b*). Gautier & Brun (1994*a*, *b*) and Gautier (1995) argued that, on several islands, a specific distribution of kinematic indicators could be seen, like on Tinos, Andros, central southern Evia, Ios and, to a lesser extent, Syros. They described the ductile deformation associated with greenschist facies metamorphism as non-coaxial, with a top-to-north (or NE) sense of shear in the northern (or northeastern) part of these islands, and a top-to-south (or SW) sense of shear in the southern (or southwestern) part. On Tinos and Andros, the domain with top-to-SW shearing is restricted to a few outcrops along the southwestern coast, so that the corresponding domes appear asymmetric with respect to the shear sense pattern (i.e. top-to-NE shearing dominates). According to Gautier & Brun (1994*a*, *b*), the sense of shear is inverted across a *c*. 1 km-wide zone trending subperpendicular to the mean stretching lineation. Within it, conjugate patterns of shear bands and symmetric boudinage structures dominate, so that this zone may be viewed as a narrow domain of coaxial strain at the transition between two domains with opposite kinematics. Further investigations on Tinos and Andros led Jolivet & Patriat (1999) to modify this description (see also Jolivet *et al.* 2004; Mehl *et al.* 2005). According to these authors, the coastal outcrops showing top-to-SW shearing should not be considered as a distinct entity but belong to a domain of coaxial strain significantly wider than previously presumed, beside the domain showing uniform top-to-NE shearing. Gautier & Brun (1994*a*, *b*) interpreted the above pattern as reflecting the dynamics of the ductile lower crust in response to isostatic rebound and dome amplification beneath a contemporaneous detachment zone (that is, the process of 'inward flow' discussed herein). A different opinion is shared by Jolivet & Patriat (1999) and Jolivet *et al.* (2004), who interpret the juxtaposed domains of coaxial and non-coaxial strain as reflecting the configuration in the middle crust, around the brittle–ductile transition zone, during early stages of extension. With further extension, the main extensional shear zones of the middle crust evolve into typical extensional detachments (Jolivet *et al.* 2004). A potential problem with this interpretation is the presence, in southern Tinos, of a large klippe (or 'extensional allochton') of the same unit that forms the hanging wall of the detachment zone in the northeastern part of the island. This klippe rests entirely onto the domain of coaxial strain defined by Jolivet & Patriat (1999). While this feature is normal in the model invoked by Gautier & Brun (1994*a*, *b*) (see also Brun & van den Driessche 1994), it is unexpected in that of Jolivet & Patriat (1999), even after a large amount of displacement is achieved along the detachment (cf. Jolivet *et al.* 2004, Fig. 13). Because well preserved eclogites and blueschists are found slightly beneath the klippe, and by analogy with the situation on Syros (see next section), Trotet *et al.* (2001*a*) and Mehl *et al.* (2005) suggested that the intervening contact represents an extensional detachment significantly older than that seen in the northeastern part of the island (at a distance of only 5 km). However, since the rocks in between belong to the same footwall unit with low-dipping foliations, this hypothesis does not readily solve the problem: the contact in the south and the northeastern detachment occupy the same structural position, therefore the former should have been reactivated (if not entirely developed) during greenschist facies shearing along the latter and is most probably connected with it. Due to this problematic issue, and on account of the numerical results obtained in this study, our opinion is that the interpretation of Gautier & Brun (1994*a*) remains a viable alternative to the one of Jolivet & Patriat (1999).

Regardless, taking into account the report of top-to-NE/ENE shearing in northern and eastern Syros during greenschist facies metamorphism (Gautier 1995; Trotet *et al.* 2001*a*; Rosenbaum *et al.* 2002), the domain of coaxial strain in southwestern Tinos strongly suggests that Tinos and Syros islands already coincided with distinct metamorphic domes during that stage of the metamorphic evolution. As a consequence, the Tinos detachment and the detachment seen in southeastern Syros, bearing a similar hangingwall rock content (Maluski *et al.* 1987; Patzak *et al.* 1994), were also probably distinct shear zones at that time (Gautier & Brun 1994*b*).

By analogy, it can be proposed that three parallel detachment systems have developed in the northwestern Cyclades during Miocene extension, coinciding with the three NW–SE-trending chains of islands seen at present, namely southern Evia–Mykonos, Gyaros–Syros, and Kea–Sifnos (Gautier & Brun 1994*a*; Jolivet *et al.* 2004). The Evia–Mykonos chain is clearly dominated by top-to-NE ductile to brittle shearing, therefore it was controlled by a NE-dipping detachment zone. In contrast, the kinematics of extensional deformation are not so clearly asymmetric in the case of the Gyaros–Syros chain. While top-to-NE/ENE shearing dominates in the eastern part of

Syros, there is no consensus among authors concerning the island as a whole. According to Trotet *et al.* (2001*a*), a continuum of top-to-ENE shearing is recorded throughout the island from the conditions of high-pressure metamorphism to those of an uneven greenschist facies overprint. A few major shear zones would have localized extensional shearing to the point that interlayered metamorphic subunits record significant differences in their pressure-temperature path (Trotet *et al.* 2001*b*). According to Trotet *et al.* (2001*a*, *b*), the same holds for Sifnos Island. While agreeing with a continuum of extensional deformation from blueschist to greenschist facies conditions, Bond *et al.* (2007) recently questioned the existence of these prominent shear zones on Syros and argued that extensional deformation was dominantly coaxial throughout the synmetamorphic exhumation history. Kinematic data reported by Gautier (1995) and Trotet *et al.* (2001*a*) do not show a dominant sense of shear on the scale of Syros Island (apart from dominantly top-to-NE/ENE shearing in the eastern part), apparently supporting the hypothesis of Bond *et al.* (2007). Finally, the southwestern chain of islands, from Kea to Sifnos, is the least known of the Cyclades (Sifnos excluded). Nevertheless, according to Walcott & White (1998) and recent work by Grasemann *et al.* (2007), Miocene top-to-SW/SSW extensional shearing dominates on Kea, Kythnos and Serifos: these three islands are, hence, probably controlled by a major SW-dipping detachment zone. In contrast, according to Trotet *et al.* (2001*a*), Sifnos displays dominantly top-to-NE extensional shearing, hence it is probably unrelated to this detachment.

In the southeastern Cyclades, no domain of coaxial deformation has been found on Naxos and Paros Islands, where extensional shearing is consistently top-to-north (Urai *et al.* 1990; Buick 1991; Gautier *et al.* 1993). Moving toward northwestern Paros, a strong (*c*. 70°) but progressive clockwise rotation of the stretching lineation is observed (Gautier *et al.* 1993), which is thought to relate to dextral shearing along the Mid-Cycladic Lineament (Gautier & Brun 1994*a*). On Ikaria, almost all kinematic data reported by Kumerics *et al.* (2005) also indicate top-to-north shearing.

In contrast, the case of Ios appears more complex. Lister *et al.* (1984) initially reported mylonitic rocks, with top-to-south kinematic indicators, which they attributed to a ductile extensional detachment named the South Cyclades shear zone. Lister *et al.* (1984) and, more recently, Vandenberg & Lister (1996) and Forster & Lister (1999) have considered that this *c*. 200 m-thick shear zone is the main structure accommodating Neogene extension on Ios. If this hypothesis is correct, then the Ios and Naxos MCCs clearly relate to two distinct (antithetic) detachment zones. However, Gautier & Brun (1994*a*) have shown that large domains with top-to-north kinematic indicators are also found in the northern limb of Ios dome. While acknowledging that the sense of shear is dominantly top-to-south on Ios (at variance with the case on most islands), Gautier & Brun (1994*b*) favoured an interpretation in which the Ios MCC formed in the footwall of a north-dipping detachment. They argued that, even in this case, the Ios and Naxos MCCs are probably related to two distinct (though synthetic) detachments, because: (1) the two domes are well defined, so that drag folding along a late normal fault in between the two islands is unlikely to have produced this division (especially since there is no evidence for such a fault in the bathymetry nor in the Messinian–Quaternary sedimentary record; and (2) pressure conditions associated with greenschist facies metamorphism are similar from southern Naxos to Ios, and are probably even lower on Antiparos, an unexpected feature in the hypothesis of a single north-dipping detachment. Therefore, along a section going from Naxos to Ios, two distinct detachment systems are required. But was Ios truly dominated by non-coaxial deformation during Miocene extension, with either a south-dipping (Lister *et al.* 1984; Forster & Lister 1999) or a north-dipping (Gautier & Brun 1994*b*) main detachment zone? The top-to-north kinematic indicators reported by Gautier & Brun (1994*a*) are associated with high-strain ductile deformation and are found both beneath and above the south-vergent South Cyclades shear zone of Lister *et al.* (1984). Vandenberg & Lister (1996) and Forster & Lister (1999) admit that top-to-north shear zones do exist in northern Ios, associated with mylonitic fabrics. Forster & Lister (1999) report these shear zones as cutting across the South Cyclades shear zone and interpret them as reflecting downdip shearing along the back-tilted flank of the MCC after significant arching of the main shear zone (cf. Reynolds & Lister 1990). This interpretation is questionable, however, because Forster & Lister (1999) indicate that these crosscutting relations are observed within augen-gneiss that occupy the core of the Ios MCC, in which the main fabric may well relate to pre-extensional events (e.g. Vandenberg & Lister 1996). Conversely, Vandenberg & Lister (1996) suggested that the South Cyclades shear zone cuts across the north-dipping detachment zone of Naxos, yet acknowledging that available geochronological data on synkinematic intrusions do not support this scenario. Altogether, these features suggest that top-to-north and top-to-south extensional shear zones on Ios are broadly contemporaneous, and that there may be no dominant sense of shear on the scale of the island during Miocene extension.

Furthermore, Vandenberg & Lister (1996) and Forster & Lister (1999) mapped a series of low-angle normal faults capping the South Cyclades shear zone, associated with chloritization and brecciation (the Ios Detachment Fault system of Forster & Lister 1999). They consider that this fault system reflects ongoing shearing along the South Cyclades shear zone during cooling and exhumation, so that the faults are reported to have the same top-to-south kinematics. However, field evidence in favour of this interpretation is scarce. The fault system is recognized mainly in the northern limb of the dome, where the normal faults dip northward and are thus assumed to have been tilted into the attitude of apparent thrust faults during subsequent arching. However, if the top-to-north ductile shear zones also developed in response to arching, as argued by Forster & Lister (1999), then arching was already effective while the rocks were still in the conditions of ductile deformation, therefore later brittle normal fault zones could hardly have rotated through the same process. We conclude that further work is needed to check whether the 'Ios Detachment Fault system' is associated with top-to-south or top-to-north kinematics.

Summarizing, like the northwestern Cyclades, the southeastern Cyclades seem to include three parallel detachment systems developed during Miocene extension, coinciding with the three east–west-trending chains of islands seen at present, namely Ikaria–Samos, Paros–Naxos, and Folegandros–Ios (Gautier & Brun 1994*a*). The two northern chains are controlled by a north-dipping detachment zone, while the deformation pattern on Ios suggests that the southern chain has no marked asymmetry. The central chain (i.e. the islands of Naxos and Paros) displays the deepest structural levels of the Cyclades, in the form of two large domes cored with migmatites (e.g. Gautier *et al.* 1993; Jolivet *et al.* 2004).

Interfering detachment systems

Using available pressure estimates for greenschist facies and locally higher temperature metamorphism and taking into account the present geometry and distribution of metamorphic domes in the Cyclades, Gautier & Brun (1994*b*) and Gautier (1995) came to the conclusion that, along at least three transects parallel to stretching (Tinos–Syros, Paros–Sikinos, Naxos–Ios), the different detachment zones and associated MCCs are partly superimposed and, therefore, probably interfere with one another. They discussed two possible evolutionary models incorporating a genetic link between successive synthetic detachment zones. A scenario was finally favoured in which a second detachment develops in the footwall of the first one, giving rise to a secondary MCC formed in the rear flank of the first one (Gautier & Brun 1994*b*, fig. 10). It is worth noting that this scenario bears some resemblance with the numerical simulations obtained in this study. Nevertheless, it has specific aspects that deserve a few comments. Firstly, the second detachment zone was thought to arise from prolonged shearing along a fault zone formed during the development of the first MCC (the 'Listric Accommodation Fault' (LAF) seen in the analogue experiments of Brun *et al.* 1994). As a result, the secondary MCC was expected to show a marked asymmetry. It is not clear whether the present numerical approach is precise enough to feature a LAF in the brittle upper crust, therefore the mechanical background for the development of a secondary MCC in the simulations may be quite different; coincidentally, we obtain no marked asymmetry for the secondary MCC. Secondly, the scenario of Gautier & Brun (1994*b*) incorporated the fact that the two MCCs should interfere, with reference to the three studied transects (for this reason, the LAF was drawn closer to the first detachment than it is in the experiments of Brun *et al.* 1994).

Gautier & Brun (1994*b*) further pointed out that, with ongoing extension, this 'second footwall detachment' scenario may ultimately result in a complete omission of the wedge of upper crustal rocks that initially formed in the rearmost part of the first MCC. They claimed that this feature compares well with the situation in the Cyclades, where no such wedge of upper crustal rocks is exposed on the islands. However, the latter point depends on the interpretation that is made of segments of the metamorphic pile exposing well-preserved eclogites and blueschists, as on Syros and Sifnos. Following the opinion of Avigad (1993) and Wijbrans *et al.* (1993) for the case of Sifnos, Trotet *et al.* (2001*a*) have proposed that high levels of the metamorphic pile on these two islands escaped pervasive retrogression because they were exhumed earlier. An apparent support to this interpretation is the fact that, on Sifnos, radiometric data from these rocks provide significantly older ages than lower levels with intense greenschist facies retrogression (Altherr *et al.* 1979; Wijbrans *et al.* 1990). As a result, high levels of the metamorphic pile may have been part of the upper crust by the time the rest of the pile underwent extensional deformation associated with greenschist facies metamorphism (Avigad 1993; Trotet *et al.* 2001*a*; Parra *et al.* 2002). If so, the claiming of Gautier & Brun (1994*b*) that no wedge of upper crustal rocks exists in the Cyclades is incorrect, and it is not so clear whether adjacent MCCs interfere or not. For instance, much of Syros would represent such upper crustal rocks, and the same may apply to Ios, where high-pressure rocks are

relatively abundant in the envelope of the dome, above the South Cyclades shear zone of Lister *et al.* (1984), displaying similarly 'old' ages as on Syros and Sifnos (van der Maar & Jansen 1983). Due to its potential implications, this hypothesis needs to be further discussed.

According to the interpretation of Trotet *et al.* (2001*a*, *b*), important extensional shear zones should exist (and are reported to do so) within the metamorphic pile of Syros and Sifnos (see also Avigad 1993). In addition, the topmost detachment fault seen in southeastern Syros, with Cretaceous metamorphic rocks in the hanging wall (Maluski *et al.* 1987) and well preserved high-pressure rocks in the near footwall, should represent a relatively old structure. However, in the case of Syros, Bond *et al.* (2007) claim that the intermediate extensional shear zones do not exist and, like other authors have argued for Sifnos and Tinos Islands (Schliestedt & Matthews 1987; Bröcker 1990; Ganor *et al.* 1996), consider that the degree of preservation of the high-pressure assemblages reflects primarily the extent of fluid infiltration during greenschist facies retrogression. Limited fluid infiltration and deformation in the least retrogressed rocks may also account for the preservation of older ages by the time rocks passed through P–T conditions of the greenschist facies, as proposed by Wijbrans *et al.* (1990) in the case of Sifnos (see however Wijbrans *et al.* 1993). This is especially clear on Tinos, where the rocks with the best preserved high-pressure assemblages (with ages around 45–37 Ma) lie at the same structural level as those showing a complete greenschist overprint (with ages around 33–21 Ma; Bröcker & Franz 1998; Parra *et al.* 2002). In this particular case, the extent of retrogression is apparently linked with the intensity of shearing during greenschist facies metamorphism (Jolivet & Patriat 1999; Parra *et al.* 2002). The same may hold for Syros (Bond *et al.* 2007) and, eventually, Sifnos (Wijbrans *et al.* 1990). Rosenbaum *et al.* (2002) also consider that, in northern Syros, at high levels of the metamorphic pile, greenschist facies overprint is localized into top-to-NE shear zones that are contemporaneous with Miocene extensional shearing in neighbouring islands. As for the detachment in southeastern Syros, its timing is poorly constrained. Trotet *et al.* (2001a) used a $^{40}Ar/^{39}Ar$ white mica age obtained close to the contact (30.3 ± 0.9 Ma; Maluski *et al.* 1987) to infer that the detachment was active at that time. Maluski *et al.* (1987) reported this age from an omphacitic metagabbro and pointed out that the obtained spectrum shows evidence for an inherited component. In addition, Trotet *et al.* (2001*a*) indicate that the actual detachment contact is marked by breccias reworking eclogites retrograded into the greenschist facies. This strongly suggests that at least part of the displacement along the detachment occurred significantly later than 30 Ma, that is, at about the same time as in other islands (e.g. Gautier & Brun 1994*a*). Altogether, the above features suggest that, in the Cyclades as a whole, well-preserved high-pressure rock assemblages represent low-strain lenses of variable size embedded into a single layer of greenschist facies metamorphism dating from the late Oligocene–early Miocene. This interpretation may apply to most islands (e.g. Wijbrans *et al.* 1990; Parra *et al.* 2002; Bond *et al.* 2007), Ios included (Forster & Lister 1999). As a result, the inference that no wedge of upper crustal rocks exists in the Cyclades (Gautier & Brun 1994*b*) remains probably valid, which, in turn, supports the view that detachment zones and associated MCCs do interfere with one another in this region. It remains that, on Syros and Sifnos, an upward gradient of preservation of the high-pressure assemblages exists across the *c*. 3 km-thick metamorphic pile (e.g. Wijbrans *et al.* 1990; Trotet *et al.* 2001*a*). We suggest that this gradient reflects the transition from pervasive deformation, below, to more localized deformation, above, within the layer of greenschist facies metamorphism. In other words, greenschist facies metamorphism in the middle crust would coincide with the broad transition from pervasive (ductile) to localized (ductile to brittle) deformation across the thickness of the crust, in good agreement with the views of Jolivet & Patriat (1999) and Jolivet *et al.* (2004).

Post-orogenic versus syn-orogenic extension

The numerical simulations presented in this paper are concerned with the case of whole-lithosphere extension. As stated above, most authors having identified extensional detachments and metamorphic core complexes in the Cyclades interpreted them as resulting from Aegean 'backarc' extension (Lister *et al.* 1984; Buick 1991; Gautier & Brun 1994*b*; Jolivet & Patriat 1999), thus apparently fitting the experimental setup. These structures developed within metamorphic rocks that previously experienced high-pressure/low-temperature conditions, therefore extension may also be described as 'late-orogenic' (Gautier & Brun 1994*b*). However, for the purpose of a comparison with the numerical results, it needs to be discussed whether the extensional structures developed strictly after crustal thickening or/and during ongoing thrusting beneath the locus of extension. In the Aegean, these two cases have been refered to as post vs. syn-thickening, or post vs. syn-collisional, extension (Gautier & Brun 1994*b*), or post vs. syn-orogenic extension/exhumation (Jolivet & Patriat 1999; Trotet *et al.* 2001*a*; Parra

et al. 2002; Jolivet *et al.* 2003), the latter terminology being now widely accepted. In the following, we prefer to use extension rather than exhumation because exhumation may also result from erosion, eventhough erosion in the Cyclades has probably been limited during the Cenozoic (e.g. Gautier & Brun 1994*a*). We emphasize that extension does not necessarily mean that the whole lithosphere, or even the whole crust, is stretched horizontally. This is obvious in the case of syn-orogenic extension, where plate convergence is the leading process and horizontal shortening the dominant regime on the lithospheric scale. Syn-orogenic extension is sometimes described as corresponding to the development of an extrusion wedge (e.g. Ring & Reischmann 2002; Ring *et al.* 2007*a*).

The distinction between post and syn-orogenic extension is a difficult task, especially because the associated faults and shear zones may have the same kinematics (Jolivet & Patriat 1999; Trotet *et al.* 2001*a*). Gautier & Brun (1994*b*) and Gautier *et al.* (1999) have argued that, because extension with a direction of stretching parallel to plate convergence was active at the same time (i.e. since at least the Aquitanian) across a wide part of the Aegean, from the Rhodope to Crete, this extension was necessarily post-orogenic, based on a comparison with the case of syn-orogenic lateral extension in the Himalaya–Tibet orogen. However, this assessment may be incorrect in the case of a significant retreat of the underthrusted slab during orogeny. As discussed by Jolivet *et al.* (2003), if the dynamics of the orogen is basically that of a retreating subduction, then extension can be everywhere parallel to convergence, including in the area lying above the frontal thrust zone. In a sense, such an orogen is not strictly collisional, therefore the description of extension as post or syn-collisional (Gautier & Brun 1994*b*) is unadapted in this case.

Even if only extensional structures are observed in a late-orogenic setting, it is usually difficult to demonstrate that their formation was strictly post-orogenic, because it can always be argued that coeval thrusting possibly occurred beneath the deepest exposed rocks. Conversely, syn-orogenic extension is demonstrated if a thrust zone can be shown to have been active while extension occurred, or had already started, at shallower levels. Avigad & Garfunkel (1989) and Avigad *et al.* (1997) tentatively argued for the latter case on Tinos and Evia islands, however their arguments have been criticized by Gautier (2000) and Bröcker & Franz (2005). Moreover, in the scenario of Avigad *et al.* (1997) for the Cyclades, coeval thrusting and inferred syn-orogenic extension are restricted to the Oligocene period, while post-orogenic extension started at about 25 Ma, associated with a pervasive greenschist facies overprint, as in the common view (see above). Avigad *et al.* (1997) also acknowledged that the identification of structures associated with the period of syn-orogenic extension is problematic.

The shape of the pressure–temperature path followed by metamorphic rocks may help to decipher between syn-orogenic and post-orogenic extension. Following Wijbrans *et al.* (1993), Jolivet and co-workers have proposed that, among the metamorphic rocks of the Cyclades, those having followed a cold geotherm during exhumation should have done so owing to syn-orogenic extension (Jolivet & Patriat 1999; Trotet *et al.* 2001*a*, *b*; Parra *et al.* 2002; Jolivet *et al.* 2003). A critical question is how cold this geotherm should be, given that exhumation beneath a detachment also helps to prevent heating. The best answer probably comes from the study of Parra *et al.* (2002), showing that, on Tinos, rocks in the footwall of the NE-dipping detachment experienced an episode of isobaric heating (a temperature increase from 400°–550 °C at about 9 kbar) between two episodes of exhumation. Parra *et al.* (2002) convincingly proposed that the first and second episodes reflect syn-orogenic and post-orogenic extension, respectively (see also Jolivet *et al.* 2004). As a result, on Tinos at least, only post-orogenic extension would be recorded since rocks moved out of the conditions of blueschist facies metamorphism. In other words, all the structures developed at greenschist facies and subsequent lower grade conditions are expected to relate to post-orogenic extension, in agreement with earlier proposals (Gautier & Brun 1994*a*; Jolivet & Patriat 1999). There does not seem to be a significant diachronism of greenschist facies metamorphism on the scale of the Cyclades (including at high levels of the metamorphic pile on Syros, see previous section), therefore the whole set of detachment zones and associated MCCs described before have probably developed during post-orogenic extension.

It is difficult to determine when this extension started. Using the data of Bröcker & Franz (1998), Parra *et al.* (2002) have suggested that the beginning of the second episode of exhumation and, therefore, the onset of post-orogenic extension in the Cyclades took place at 30 Ma (see also Jolivet *et al.* 2003, 2004). Based on the data of Wijbrans *et al.* (1990), Wijbrans *et al.* (1993) have proposed a P–T path for lower levels of the metamorphic pile on Sifnos that resembles the one of Parra *et al.* (2002) for Tinos. However, in this case, isobaric heating (at 6.5 kbar) would have occurred from 30 Ma to 22 Ma, so that the second episode of exhumation would start at 22 Ma. Nevertheless, the scenario of Wijbrans *et al.* (1993) assumes that post-thickening extension started at 30 Ma, being first confined to

crustal levels beneath the presently exposed rock pile, then migrating into this pile. Therefore, both interpretations (Wijbrans *et al.* 1993; Parra *et al.* 2002) concur in the idea that post-orogenic extension was active in the Cyclades during the earliest Miocene (e.g. Gautier & Brun 1994*a*); they even suggest that it was already active during the late Oligocene.

In contrast, Ring and co-workers have put forward an extreme alternative scenario, in which a context of syn-orogenic extension would have been maintained in the Cyclades until *c*. 21 Ma (Ring *et al.* 2001; Ring & Reischmann 2002; Ring & Layer 2003; Ring *et al.* 2007*a*). This would have been followed by an episode of post-orogenic extension starting later than *c*. 15 Ma (Ring *et al.* 2007*a*), probably at *c*. 12 Ma (Ring & Layer 2003), and resulting from thermal weakening at the time the Aegean magmatic arc would have reached the Cyclades. If this scenario is correct, then extensional structures associated with greenschist facies and higher temperature metamorphism should largely date from an episode of syn-orogenic extension, as, for instance, on Naxos (e.g. Gautier *et al.* 1993; Keay *et al.* 2001), Tinos (e.g. Gautier & Brun 1994*a*; Bröcker & Franz 1998, 2000; Jolivet *et al.* 2004) and Andros (Gautier & Brun 1994*b*; Bröcker & Franz 2006). As a result, our attempt to compare our numerical simulations and the Cycladic case would be questionable.

According to Ring and co-workers, the Central Aegean region is floored by the poorly exposed parautochtonous Basal unit, coinciding with the Almyropotamos unit in central southern Evia (e.g. Dubois & Bignot 1979); this unit would have been underthrusted while extensional shearing developed at higher levels of the metamorphic pile. This interpretation follows Avigad *et al.* (1997) except for the timing of the episode of syn-orogenic extension (before about 25 Ma for Avigad *et al.* as late as 21 Ma for Ring and co-workers). We think that this scenario is unlikely, especially its timing, for the three following reasons:

- Rb–Sr and $^{40}Ar/^{39}Ar$ dating of phengites from samples of the Basal unit has yielded ages mostly between 21 and 24 Ma (Ring *et al.* 2001; Ring & Reischmann 2002; Ring & Layer 2003). While they coincide with the timing of greenschist facies metamorphism in the overlying unit, these ages were interpreted as reflecting high-pressure metamorphism in the Basal unit (hence constraining the age of underthrusting) because the dated phengites have a high Si content ($\geq$3.3 per formula unit). However, as thoroughly discussed by Bröcker *et al.* (2004) and Bröcker & Franz (2005), this interpretation is questionable and the obtained ages are more likely to reflect the timing of post-high-pressure greenschist facies retrogression, as in the overlying unit. Further support to the objections of Bröcker *et al.* (2004) is found in the recent Rb–Sr study of Wegmann (2006) on rocks from south-easternmost Evia, at higher levels of the metamorphic pile, far above the Basal unit. In one rock repeatedly dated with a microsampling method, phengites have a Si content ranging from 3.36 to 3.74 pfu and yield Rb–Sr ages ranging from 21 to 11 Ma. Following the line of reasoning of Ring and co-workers, this would mean that higher levels of the metamorphic pile were still experiencing high-pressure conditions at that time. This is at odds with the report from the neighbouring northwestern Cyclades (Bröcker & Franz 1998, 2006) and from southern Evia itself where, according to Ring *et al.* (2007*a*), such rocks experienced greenschist facies conditions as early as 21 Ma. It should also be stressed that the youngest fossils found so far in the Almyropotamos unit represent the lower or middle Eocene (Dubois & Bignot 1979), not the upper Eocene–Oligocene as commonly reported (e.g. Ring *et al.* 2007*a*), therefore this unit may have started to underthrust as early as during the early Eocene;
- According to the scenario of Ring and co-workers, the Central Aegean region should have been characterized by a depressed geotherm as late as around 21 Ma (i.e. as long as underthrusting and inferred high-pressure metamorphism were developing), and no significant thermal overprint is expected before about 14 Ma, when arc magmatism is considered to have reached the Cyclades. However, this does not take into account the case of the migmatite domes on Naxos and Paros Islands. U–Pb dating of zircons from the migmatitic core of Naxos indicates that partial melting mostly occurred at *c*. 17.5 Ma and was already under way at 20 Ma (Keay *et al.* 2001), in good agreement with time constraints provided by other radiometric methods (e.g. Andriessen *et al.* 1979; Wijbrans & McDougall 1988). This shows that at least part of the Central Aegean region was actually characterized by a high geotherm at about 20 Ma. The Basal unit is unlikely to lie underneath the migmatite domes, because if it had been underthrusted until 21 Ma, migmatization in the hanging wall of this thrust could hardly have been maintained until *c*. 17 Ma (cf. Keay *et al.* 2001). Hence, the migmatite domes probably cut across the contact and, as stated before,

represent the deepest structural levels of the Cyclades. It is not known whether the migmatites seen on Naxos and Paros expand laterally beneath the other islands, although there are chemical data to suggest so (Gautier & Brun 1994*a*). Regardless, the area of Naxos and Paros was hot at 20 Ma, and we do not see how this can be reconciled with the hypothesis of regional underthrusting as late as 21 Ma; and

- Post-orogenic extension is accompanied by the formation of grabens (as also illustrated by our numerical experiments) which may evolve into supra-detachment basins. Thus, the base of the supradetachment basin stratigraphy may provide a minimum age for the onset of post-orogenic extension. The oldest supra-detachment sediments known in the Cyclades, on Naxos and Paros, are Aquitanian (23.0–20.4 Ma; Lourens *et al.* 2004) and form the basis of a nearly continuous stratigraphy reaching the upper Miocene (Angelier *et al.* 1978; Roesler 1978; Sanchez-Gomez *et al.* 2002). This documents continuous formation of accomodation space from the Aquitanian onward, suggesting no fundamental change in the tectonic setting since that time (Gautier *et al.* 1993; Gautier & Brun 1994a; Sánchez-Gómez *et al.* 2002). In addition, the Aquitanian and Burdigalian sediments are marine deposits (e.g. Angelier *et al.* 1978), while it may be argued that sedimentation beneath sea level is unexpected during (or immediately after) an episode of extension coeval with underthrusting, as in the scenario of Ring et co-workers.

To conclude on this part, our opinion is that a context of syn-orogenic extension could hardly have existed in the Cyclades later than about 25 Ma, considering that at least a few million years are necessary to enhance partial melting after underthrusting, whatever the exact origin of the heating event. Syn-orogenic extension finishing at *c*. 37 Ma, as suggested by Parra *et al.* (2002), would fit this condition. We also note that the onset of post-orogenic extension at *c*. 30 Ma in the Cyclades, as suggested by Wijbrans *et al.* (1993) and Parra *et al.* (2002), is fully compatible with the timing of events reported by Thomson & Ring (2006) and Ring *et al.* (2007*b*) in the nearby Menderes massif, where the allochtonous position of the 'blueschist' unit of the Cyclades is well established.

Did extension in the Cyclades significantly deviate from plane strain deformation?

Finally, before comparing the Cyclades and our numerical experiments, we should examine whether crustal extension in the Cyclades closely approximated plane strain deformation, as assumed when extrapolating the two-dimensional simulations to a three-dimensional setting, or not. Based on the presence of folds with axes parallel to the mean stretching lineation on several islands (Naxos, Paros, Tinos and Andros), some authors have argued that a significant component of transverse (*c*. east–west) shortening has accompanied MCC-type extension in the Cyclades (Urai *et al.* 1990; Buick 1991; Avigad *et al.* 2001; Jolivet *et al.* 2004). According to Avigad *et al.* (2001), the magnitude of this lateral contraction was high enough to maintain the thickness of the crust roughly constant despite intense extensional deformation. Transverse shortening may be viewed as a normal response to the three-dimensional displacement field of the Aegean lithosphere during extensional spreading (Gautier *et al.* 1999; Jolivet *et al.* 2004), nevertheless our opinion is that its contribution to crustal strain has never been significant in the Cyclades. Most of the folds taken as evidence for strong lateral shortening are either isoclinal to tight folds with low-dipping axial planes subparallel to the main foliation (therefore they do not properly document horizontal shortening) or upright open folds (documenting limited shortening). On Naxos, which is reported as the island where transverse shortening is best seen, Vanderhaeghe (2004) has shown that subvertical granitic dikes have emplaced throughout the inner envelope of the migmatite dome during extension. About one half of these dikes trend parallel to the *c*. north–south stretching lineation and another half perpendicular to it, therefore bulk flattening strain and horizontal stretching in the east–west direction are actually documented (Vanderhaeghe 2004). The relatively steep attitude of foliations within and around the migmatitic core of the Naxos dome may reflect the diapiric ascent of the migmatites (Vanderhaeghe 2004) rather than folding and horizontal shortening (e.g. Jolivet *et al.* 2004).

In analogue experiments simulating the spreading of a weak lithosphere toward a free boundary, transverse shortening is present but is confined to the inner (northern in an Aegean frame) part of the deforming sheet (Gautier *et al.* 1999). The Cyclades are unlikely to have occupied such a inner position during Aegean extension, at least until the late Miocene, therefore the lack of clear evidence for significant transverse shortening in the ductile record of the islands is not surprising. The situation is possibly different since around the Pliocene (since <3 Ma according to Gautier *et al.* 1999, but more probably since <8 Ma according to the paleomagnetic results of van Hinsbergen *et al.* 2005*b*), when a southward jump of the northwestern tip of the Aegean arc brought the Cyclades in a more

inner position than they were before, and when the westward extrusion of Anatolia started to affect the evolution of the Aegean domain. This regional reorganization probably explains the record of WNW–ENE shortening (in the form of tight folds, strike-slip and reverse faults) in Neogene sediments of the Central Aegean region (Angelier 1977*b*), some of which must be younger than 10 Ma (Sánchez-Gómez *et al.* 2002).

We conclude that crustal extension in the Cyclades probably coincided with near-plane strain deformation during much of the period of post-orogenic extension (i.e. except possibly since < 8 Ma), therefore comparing the evolution of the Cyclades with our two-dimensional experiments bears some logic.

Comparison and discussion

Comparison between the numerical experiments and the Cyclades

The previous overview has shown that several aspects of the tectonic evolution of the Cyclades during the Neogene are reminescent of the results of our numerical experiments, especially the coexistence of several MCCs and associated detachment systems along a section parallel to extension ('How many MCC and detachment systems in the Cyclades?' section) and the fact that at least some of these MCCs interfere with one another ('Interfering detachment systems' section). In addition, we have shown that the general kinematic framework that prevailed during the development of these structures is comparable to the one in our experimental setup, that is, a context of whole-lithosphere (i.e. post-orogenic) extension ('Post-orogenic vs. syn-orogenic extension' section) associated with near-plane strain deformation (previous section). We now compare in more detail the results of our numerical experiments with the geological record of the Cyclades. Four essential issues are compared: the final depth of the Moho, the geometry of MCCs, their kinematic pattern, and the amount of time associated with their exhumation:

Moho depth. In the experiments, the Moho interface remains nearly flat throughout the extensional process (Fig. 5). The final Moho depth increases with increasing initial crustal thickness and with decreasing boundary velocity (Fig. 7). Within the range of conditions giving rise to interfering MCCs (see 'Numerical experiments' section), this depth varies between 22.5 and 29 km. In the Cyclades, various geophysical investigations indicate that the Moho is almost flat, lying at depths around 25–26 km (Makris & Vees 1977; Makris 1978; Vigner 2002; Li *et al.* 2003; Tirel *et al.* 2004*b*), well within the expected range of values. According to the experiments, a value of 25–26 km is compatible with an initial crustal thickness (at the onset of post-orogenic extension) of *c.* 43–44 km (Fig. 7e) and a boundary velocity of *c.* 2.0–2.3 cm/a (Fig. 7f).

Geometry of MCCs. Before comparing the geometry (this section) and kinematic pattern (next section) of MCCs in the numerical simulations and in the Cyclades, it must be stressed that, unlike in the experimental setup, the crust of the Cyclades was neither homogeneous nor isotropic at the onset of post-orogenic extension. Most authors agree on the view that crustal thickening during the earlier orogenic period occurred through the operation of dominantly SSW-vergent thrusts (e.g. Bonneau 1982; Jolivet *et al.* 2003; van Hinsbergen *et al.* 2005*a*). It may be suspected that some of these thrusts were later reactivated as normal-sense detachment zones (e.g. Gautier *et al.* 1993; Avigad *et al.* 1997; Trotet *et al.* 2001*a*; Jolivet *et al.* 2003; Ring *et al.* 2007*a*), which may account for the predominance of top-to-NNE shearing during extension on the scale of the Cyclades. However, clear evidence that earlier thrusts have particularly localized later extensional shearing is missing. On Ios Island, Vandenberg & Lister (1996) suggested that the south-vergent South Cyclades shear zone partly reactivates (in extension) a north-vergent Alpine thrust, however the arguments for such a thrust are unclear. It remains that dominantly SSW-vergent Alpine thrusting has certainly produced a broadly north-dipping stack of various lithologies, the weakest of which may have localized later extensional shearing. Thus, not only the predominance of top-to-NNE shearing during extension might be explained by earlier thrusting, so does the spatial distribution of extensional detachments, which could in part reflect the initial geometry of the thrust stack. We are aware of this problem when comparing the Cyclades with the numerical simulations, the problem arising from our deliberate choice of the simplest possible initial conditions in the experimental setup.

Nevertheless, as the simulations compare relatively well with the natural case, our impression is that the role of pre-existing structures has been minor during post-orogenic extension in the Cyclades. We suspect that this arises from the high thermal profile of the crust at, or soon after, the initiation of post-orogenic extension. According to our experiments, at least the lower half of the crust was at temperatures in excess of 550 °C, at which the viscosity contrast between the most common rock types is severely reduced. At these levels, the most significant viscosity drops relate

to the progress of anatexis, which depends only partly on the geometry of earlier thrusting.

A number of observations imply that several MCCs coexist in the Cyclades (see 'How many MCC . . .' section). Structural data suggest that three detachment systems and associated MCCs have developed in both the northwerstern Cyclades (coinciding with the Evia–Mykonos, Gyaros–Syros and Kea–Sifnos island chains) and the southeastern Cyclades (coinciding with the Ikaria–Samos, Paros–Naxos and Folegandros–Ios island chains). As discussed by Gautier & Brun (1994*b*), the MCCs of at least two of these chains apparently interfere with one another, based on the relationships between Naxos and Ios, Paros and Sikinos, and Tinos and Syros (see 'Interfering detachment systems' section). We now focus on a comparison between the numerical simulations and the Naxos–Ios and Tinos–Syros island pairs, leaving Paros–Sikinos aside because it repeats the case of Naxos–Ios without an equivalent structural or geochronological dataset being available.

We find striking similarities between the simulations and the selected island pairs in terms of geometry (Fig. 9). Naxos constitues a large MCC with a pronounced asymmetry, exhuming high-temperature lower crustal rocks (e.g. Gautier *et al.* 1993). Ios constitutes another MCC (e.g. Vandenberg & Lister 1996) formed in the direction opposite to the slope of the Naxos detachment. The Ios dome seems symmetric (at least, its asymmetry is not as pronounced as on Naxos or Paros). It is appparently narrower than the Naxos dome (although both are partly hidden beneath sea level) and exposes lower grade rocks (e.g. van der Maar & Jansen 1983), indicating that the Ios MCC is less developed. The Ios dome is superimposed on the southern flank of the Naxos dome (Gautier & Brun 1994*b*). Although less clearly expressed, the Tinos–Syros island pair displays a similar geometry. Tinos is an asymmetric MCC exhuming rocks with a pervasive greenschist facies overprint (Gautier & Brun 1994*a*; Jolivet & Patriat 1999; Parra *et al.* 2002). Syros is another MCC formed in the direction opposite to the slope of the Tinos detachment. However, Syros does not show a regular dome, which may be due to the moderate size of the island and to the influence of large normal faults cutting across the metamorphic series (Ridley 1984). It exposes rocks with broadly a less intense greenschist facies overprint than on Tinos (e.g. Trotet *et al.* 2001*a*). We have discussed in the 'Interfering detachment systems' section the possible interpretations of this feature, suggesting that the upward gradient of preservation of the high-pressure assemblages across the metamorphic pile of Syros (and Sifnos) may reflect the transition from pervasive deformation, below, to more localized deformation, above, within a coherent layer of greenschist facies metamorphism. If so, then at least part of Syros exposes rocks of slightly shallower origin than on Tinos. This hypothesis is supported by a comparison of the P–T paths of the deepest rocks on Syros (Trotet *et al.* 2001*b*) and Tinos (Parra *et al.* 2002), showing that, along the greenschist facies segment of the exhumation path, temperatures were $\geq 50^{\circ}$ higher in the case of

	IOS	NAXOS
shape of the MCC	symmetric dome	asymmetric dome
kinematics of extension	no dominant sense (?)	top-to-north
post-HP highest metamorphic grade	greenschist	anatexis
radiometric record of extension	~ 20-13 Ma	>20-10 Ma
main period of exhumation	?	17-12 Ma
	SYROS	**TINOS**
shape of the MCC	domal ?	asymmetric dome
kinematics of extension	no dominant sense (?)	top-to-northeast
post-HP highest metamorphic grade	greenschist	greenschist (T>50°C or more / Syros)
radiometric record of extension	~ <30-11 Ma	22-11 Ma
main period of exhumation	?	22-15 Ma (?)

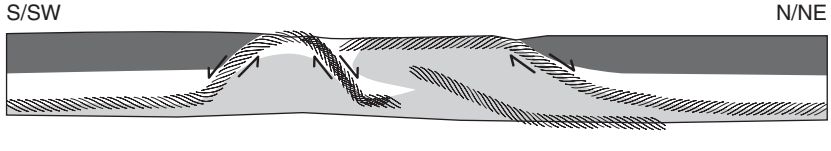

Fig. 9. Comparison between a crustal-scale cross-section showing interfering MCCs, as deduced from the numerical analysis, and relevant data from two transects in the Cyclades showing closely spaced MCCs, as discussed in the text. The comparison reveals a good agreement.

Tinos. In our experiments, the isotherms are carried upward during the earlier stages of MCC development, therefore we expect a rock of deeper origin to experience higher temperatures during exhumation, as also clearly illustrated by the numerical experiments of Gessner *et al.* (2007). Thus, the Tinos MCC has apparently accommodated more exhumation than the Syros MCC has. Note that the same process of upward heat transport during MCC development might also account for the different P–T paths obtained by Trotet *et al.* (2001*b*) across the metamorphic pile of Syros and Sifnos (see e.g. Gessner *et al.* 2007, Fig. 6). As discussed by Gautier & Brun (1994*b*), the Syros MCC is probably superimposed on the southwestern flank of the Tinos MCC.

Summing up, the geometry of MCCs along the Naxos–Ios transect and, to a less extent, the Tinos–Syros transect, compares well with the numerical simulations (Fig. 9). The comparison is more convincing with type 2 experiment, in which the second dome develops in the immediate vicinity of the first dome, so that the two MCCs are partly superimposed (Figs 5d, e, f and 6). In this case, no wedge of upper crustal rock is preserved between the MCCs, a feature that Gautier & Brun (1994b) have claimed to characterize the Cyclades. If, alternatively, higher levels of the metamorphic pile on Syros (and Sifnos) represent rocks that were exhumed to upper crustal conditions before the onset of post-orogenic extension (e.g. Trotet *et al.* 2001*a*; see discussion in 'Interfering detachment systems' section), then the structure is broadly the same, with only the Syros MCC being less developed (i.e., leaving a cap of upper crustal rocks near the apex of the dome).

In addition, special attention should be paid to the width of the two largest MCCs of the Cyclades, on Naxos and Paros. According to the above comparison, these two domes represent MCCs of the first generation. In the experiments, depending on the initial conditions, the width of the first dome is quite variable (Fig. 7a, b). The width of Naxos and Paros domes, measured in the same way as in the experiments (from the front of the detachment, plunging northward, to the rearmost part of the dome, before reaching a wedge of brittle upper crust) is at least 35 km and most probably less than 60 km. This range is compatible with an initial crustal thickness between *c*. 41 and 44 km, and seems to exclude greater values (Fig. 7a). It also seems to exclude a boundary velocity lower than *c*. 2 cm/a (Fig. 7b). Thus, the width of the MCCs of the first generation suggests broadly the same range of initial conditions as the final Moho depth does (see 'Moho depth' section).

Kinematic pattern. Similarities are also found between the simulations and the Naxos–Ios and Tinos–Syros island pairs in terms of kinematic development of the MCCs. However, before attempting a comparison, we should keep in mind the origin of shear zones in the numerical experiments, and address the question whether the same process could have operated in the Cyclades. In the experiments, faulting occurs in the upper crust due to the imposed horizontal stretching; a major fault (i.e., a detachment) ultimately develops at this level if stretching is strong enough (see 'Analysis of the two experiments' section; see also Tirel *et al.* 2004*a*). In the lower crust, ductile shear zones develop as a by-product of the process of inward flow. In the Cyclades, Gautier and Brun (1994*a*, *b*) have interpreted the shear zone pattern of some of the islands (especially Tinos, Andros, Ios) as reflecting such a process of inward flow (see 'How many MCC…' section). On Tinos and Andros, there is good evidence that this shear zone pattern developed during greenschist facies metamorphism and subsequent cooling to conditions corresponding to the transition from pervasive ductile to localized semi-brittle behaviour (Gautier & Brun 1994*a*; Gautier 1995; Jolivet & Patriat 1999; Jolivet *et al.* 2004; Mehl *et al.* 2005). In our experiments, shearing due to inward flow occurs significantly below the ductile–brittle transition (i.e., at temperatures at least *c*. 150 °C higher than the temperature of *c*. 300 °C obtained for the transition), nevertheless it is conceivable that shearing may propagate up to this interface if the ductile–brittle transition is to become a low-strength horizon after a certain amount of crustal extension is achieved (see 'Analysis of the two experiments' section). The structural record on Tinos and Andros shows that this situation may hold in the Cyclades. In addition, as micaschists and marbles dominate among the various rock types found in the islands, shearing due to inward flow may propagate at even shallower depths (that is, along an isotherm of less than 300 °C) if the proper rheological laws were used, instead of that of quartz-diorite. Nevertheless, orthogneisses apparently dominate at lower levels of the Cyclades rock pile, as seen on Naxos, Paros and Ios (e.g. van der Maar & Jansen 1983; Gautier *et al.* 1993), therefore the choice of quartz diorite as the representative rock type for the Central Aegean crust as a whole seems justified (see also Jolivet *et al.* 2003, 2004).

As mentioned before, Naxos and Paros Islands are asymmetric domes that consistently display top-to-north shear criteria. These kinematics are observed from the envelope of the domes (Gautier *et al.* 1993) down to the migmatitic core of Naxos (Buick 1991) and the poorly defined migmatitic domain of Paros (Gautier *et al.* 1993). Hence, in

the Cyclades, the largest MCCs, associated with the most pronounced exhumation, do not display evidence of inward flow emanating from the rear part of the dome (that is, inward flow that would produce shearing antithetic to the main detachment zone) whereas, according to the interpretation of Gautier & Brun (1994*a*, *b*), less mature MCCs do so. This may be viewed as a paradox, however, the present experiments show that it is not. As seen on Figure 5, SZ1, which relates to this antithetic inward flow toward the main dome, is pronounced but confined to great depths and, unlike SZ2, never reaches the surface. In contrast, in the case of the secondary dome, the two limbs coincide with antithetic shear zones that extend upward the two flat-lying shear zones (SZ11 and SZ12) developed in response to renewed inward flow. As a consequence, the secondary dome tends to be symmetric, and it can be expected that no dominant sense of shear will be found around its apex. These features compare relatively well with the case of Ios and Syros Islands (see 'How many MCC…' section). As mentioned in 'Analysis of the two experiments' section, SZ12 reactivates SZ1 in opposite sense but with less strain accumulated, therefore it can be expected that relics of the first kinematics will be found along SZ12. While assuming that the Ios MCC was controlled by a north-dipping detachment, Gautier & Brun (1994*b*) suggested that this feature may explain the predominance of top-to-south shearing across the Ios dome (that is, top-to-south shearing would in part reflect early inward flow in the rear flank of the Naxos MCC). However, because the relations between top-to-south and top-to-north shearing are unclear on Ios (see 'How many MCC…' section), we leave it open whether this hypothesis makes sense. The same applies to Syros, which is possibly dominated by coaxial deformation, but where there is no indication of an early top-to-SW shearing event that would be overprinted by top-to-NE shearing (e.g. Trotet *et al.* 2001*a*; see 'How many MCC…' section).

Summarizing, both the geometry (cf. previous section) and the kinematic pattern of MCCs compare well between the experiments and the Naxos–Ios and Tinos–Syros island pairs (Fig. 9). In both cases, the comparison holds for two among three chains of islands, and, thus, seems to ignore the Ikaria–Samos and Kea–Sifnos chains. It should be reminded that, in the experiments with interfering MCCs, additional MCCs do develop (see 'Description of two experiments' section), located at far distance from the MCCs under discussion, so that the former do not interfere with the latter (i.e. they are not superimposed nor they rework earlier shear zones). We tentatively suggest that the Ikaria–Samos and Kea–Sifnos chains, which lie relatively far from the other chains, coincide with these non-interfering MCCs.

Timing of exhumation. The simulations and the Cyclades are now compared in terms of chronology using two approaches. Firstly, the comparison may concern the total time elapsed from the onset of post-orogenic extension until the time the development of all MCCs has reached an end. The latter bound is not equivalent to the end of the extensional process because lithospheric stretching may persist due to unchanged boundary conditions. However, due to crustal thinning, the style of extension is expected to change, and the development of MCCs to be arrested (e.g. Buck 1991), which is indeed what we observe in the experiments (see also Tirel *et al.* 2008). The amount of time defined in this way is here termed the duration of MCC-type extension. In the experiments, within the range of conditions giving rise to interfering MCCs, the duration of MCC-type extension varies between 16 and 32 Ma (Fig. 7). In the Cyclades, it can be estimated as follows: for the onset of post-orogenic extension, following the discussion in 'Post-orogenic vs. syn-orogenic extension' section, we take 30 Ma (e.g. Parra *et al.* 2002; Jolivet *et al.* 2004) as the earliest possible date, which is consistent with the record in the nearby Menderes massif (Thomson & Ring 2006; Ring *et al.* 2007*b*). The latest possible date is *c.* 23 Ma (Gautier & Brun 1994*a*; Bröcker & Franz 1998, 2005, 2006). As for the end of MCC-type extension, a change in structural style seems indeed recorded in the Cyclades during the late Miocene, when regional-scale high-angle faulting, bounding Messinian–Quaternary basins, succeeded to fast cooling of the metamorphic domes, vanishing in the time range *c.* 11–6 Ma (Gautier & Brun 1994*a*; Sánchez-Gómez *et al.* 2002; Hejl *et al.* 2002, 2003; Kumerics *et al.* 2005; Iglseder *et al.* 2006; Brichau *et al.* 2006, 2007). This is in line with the Messinian age for the oldest sediments nonconformably covering the metamorphic series on Milos (van Hinsbergen *et al.* 2004). We thus set the end of MCC-type extension in between 11 and 6 Ma. It is worth noting that the youngest evidence of fast cooling in the footwall of a low-dipping detachment is provided by islands largely made up of a young I-type intrusion, like Ikaria, Serifos, Mykonos and the western part of Naxos (Altherr *et al.* 1982; Hejl *et al.* 2002, 2003; Kumerics *et al.* 2005; Iglseder *et al.* 2006; Brichau *et al.* 2006). It is therefore possible that arc magmatism locally had the capacity of delaying the end of MCC-type extension by a few million years, although Brichau *et al.* (2006) argue that, on Naxos, the intrusion of the *c.* 12 Ma-old granodiorite had a negligible effect on the kinetics of the detachment system. Combining the above dates, the

duration of MCC-type extension in the Cyclades is between 12 and 24 Ma, in good agreement with the experimental range. It is compatible with any initial crustal thickness in the range of 40–50 km (Fig. 7c) while it seems to exclude a boundary velocity lower than *c*. 1.7 cm/a (Fig. 7d).

Secondly, the comparison may concern the relative timing of MCC development along a section parallel to stretching, as in the case of the Naxos–Ios and Tinos–Syros island pairs. In the experiments (and in the scenario favoured by Gautier & Brun 1994*b*), the second dome starts to develop once the first dome has achieved much of its exhumation (Fig. 5). This suggests that the period of fastest cooling in the first dome should predate that in the second dome. For instance, in Figure 5a, the first dome experiences fast cooling between the time slices 7.0 Ma and 11.4 Ma, while the second dome does so later, until about 17.4 Ma. At first sight, this relation seems to imply that cooling ages should be older in the first dome. However, this is not necessarily correct, because the amount of exhumation is also different between the two domes. In Figure 5a, at 7.0 Ma, the green layer is approximately bounded by the isotherms 350 and 550 °C, therefore it represents rocks in greenschist facies conditions. Rb–Sr white mica ages from this layer would normally date this stage at 7.0 Ma. Considering the range of estimates for the closure temperature of argon in white mica, between about 330 and 450 °C (e.g. Wijbrans & McDougall 1988; Kirschner *et al.* 1996), $^{40}Ar/^{39}Ar$ white mica ages from this layer should also broadly date the stage at 7 Ma, or possibly the stage at 11.4 Ma, when at least the upper half of the green layer lies above the 350 °C isotherm. In the first dome, the greenschist facies layer, together with deeper rocks, are fastly exhumed within the same time range, from 7.0 to 11.4 Ma. The same relations are observed in Type 2 experiment. At the end of MCC-type extension, especially in Type 2 experiment (Fig. 5d), the second dome exposes only rocks of the greenschist facies layer, therefore white mica ages from this dome are expected to be not significantly different from white mica ages and higher temperature chronometers (e.g. U–Pb on zircon, $^{40}Ar/^{39}Ar$ on hornblende) from the first dome (e.g. in Fig. 5, within the time range from 7.0 to 11.4 Ma, i.e. within ≤ 4.4 Ma). Moreover, Figure 5b shows that, at the same time the second dome rises, shearing is still active along the frontal detachment of the first dome (cf. the stage 17.4 Ma). Hence, cooling ages from this frontal segment of the first dome are expected to be as young as the cooling ages of the second dome. Altogether, these relations suggest that there is not necessarily a significant difference to be expected in the geochronological record of the two domes. The only marked difference should concern the period of fastest cooling, however it is possible that the second dome does not raise enough to allow a proper documentation of this fast cooling period on geochronological grounds.

On Naxos, a period of fast cooling is recorded in the migmatitic core and amphibolite facies inner envelope of the dome in between ca. 16 and 8 Ma (Wijbrans & McDougall 1988; Gautier *et al.* 1993), following an anatectic event that lasted from at least 20 Ma until *c*. 17 Ma (Keay *et al.* 2001). The period of fastest exhumation probably occurred between the end of the anatectic event and the emplacement of the Western Naxos Granodiorite (Gautier *et al.* 1993), that is, beween about 17 and 12 Ma according to the data of Keay *et al.* (2001). S-type granites emplaced in the inner envelope of the dome at 15.5–12 Ma (Keay *et al.* 2001), possibly as a result of decompression melting at deeper levels of the rock pile during fast exhumation. Ongoing core complex development after 12 Ma is indicated by the syn-kinematic character of the Western Naxos Granodiorite with respect to the north-dipping detachment zone, and by the subsequent development of massive cataclasites along the contact between the two (Urai *et al.* 1990; Buick 1991; Gautier *et al.* 1993). A pseudotachylite vein from this contact is dated at 10 Ma (Andriessen *et al.* 1979). According to Brichau *et al.* (2006), brittle shearing along the detachment occurred as late as 8.2 ± 1.2 Ma, based on low-temperature thermochronology. As mentioned above, the intrusion of a large amount of arc-related magma (i.e. the Western Naxos Granodiorite) may have sustained the development of the Naxos MCC for a longer time, although this is not the hypothesis favoured by Brichau *et al.* (2006). As a fact, the two youngest ages obtained by Brichau *et al.* (2006) come from the northern part of the metamorphic dome, seemingly far from the granodiorite. This area also yields the youngest K–Ar and $^{40}Ar/^{39}Ar$ hornblende and biotite ages from the dome (Andriessen *et al.* 1979; Wijbrans & McDougall 1988), a feature that it is tempting to attribute to progressive northward migration of unroofing in the footwall of the detachment (Gautier *et al.* 1993; Brichau *et al.* 2006). However, this could also result from the emplacement of the Western Naxos Granodiorite or an equivalent young intrusion beneath this area, as proposed by Andriessen *et al.* (1979), Wijbrans & McDougall (1988) and Keay *et al.* (2001). Such an intrusion actually exists, as indicated by the local occurrence in northernmost Naxos of a hornblende-bearing I-type granite dated at *c*. 12 Ma (Keay *et al.* 2001). Hence, it is possible that ongoing development of the Naxos MCC after 12 Ma has occurred owing to the emplacement of arc-related magmas.

In the rear part of the dome, rocks that did not experience temperatures higher than 550 °C were at about 500 °C at *c*. 22.5–20 Ma and cooled to about 300 °C at *c*. 14–11 Ma (Andriessen *et al.* 1979; Wijbrans & McDougall 1988; Andriessen 1991).

The cooling history of the Ios MCC is not well constrained. A $^{40}Ar/^{39}Ar$ white mica pseudo-plateau age at about 20.5 Ma is considered to date shearing along the South Cyclades shear zone (Baldwin & Lister 1998). A Rb-Sr white mica age from a deformed aplitic vein at 13.2 ± 0.4 Ma (Henjes-Kunst & Kreuzer 1982) together with $^{40}Ar/^{39}Ar$ potassium feldspar minimum apparent ages at about 14 Ma from mylonitic augengneiss (Baldwin & Lister 1998) date another (distinct?) shearing event (vandenberg & Lister 1996; Baldwin & Lister 1998). This second event is suspected to reflect the influence of the mid-Miocene magmatism of the Cyclades, yet, so far, there is no clear evidence for any Miocene intrusion on Ios. Hence, the ages at 13–14 Ma may relate to deformation without a specific thermal event. Apatite fission track ages indicate cooling below about 100 °C between 13.3 ± 1.1 and 8.3 ± 1.1 Ma (Hejl *et al.* 2003). Comparing the geochronological record on Naxos and Ios, we find no significant diachronism. As explained above, because the Ios MCC is associated with much less exhumation, this observation is not incompatible with the Ios dome having formed later.

On Tinos, $^{40}Ar/^{39}Ar$ and Rb–Sr ages on white mica indicate that greenschist facies top-to-NE extensional shearing occurred at about 24–21 Ma (Bröcker & Franz 1998, 2005). The detachment zone is crosscut by the Tinos composite intrusion and associated thermal aureole (Altherr *et al.* 1982; Avigad & Garfunkel 1989; Bröcker & Franz 2000). Rb–Sr and K–Ar ages from the main I-type granite (Altherr *et al.* 1982; Avigad *et al.* 1998) and its thermal aureole (Bröcker & Franz 2000) suggest an early cooling at 15.5–14 Ma. Whole-rock Rb–Sr dating indicates that marginal S-type intrusions emplaced at the same time (Altherr *et al.* 1982; Bröcker & Franz 1998). Altherr *et al.* (1982) originally argued that the main granite probably emplaced before 17 Ma, however available radiometric data are compatible with the view that it did so at around 15 Ma (see discussion in Bröcker & Franz 2000). Recent U–Pb dating of zircons from the main intrusion has yielded an age of 14.6 ± 0.2 Ma (Brichau *et al.* 2007), supporting the latter view. On the one hand, this indicates that much of the displacement along the detachment zone occurred before 15 Ma. On the other hand, the margins of the plutonic complex show evidence of top-to-NE shearing during and subsequent to emplacement (Gautier & Brun 1994*a*; Bröcker & Franz 1998; Jolivet & Patriat 1999; Brichau *et al.* 2007). A series of subvertical NW–SE-trending dykes dated at 12–11 Ma (Avigad *et al.* 1998) documents ongoing NE–SW stretching once the rocks reached the brittle upper crust (see also Mehl *et al.* 2005). Final cooling at around 12–9 Ma is documented by apatite fission track ages from the main intrusion (Altherr *et al.* 1982; Hejl *et al.* 2002; Brichau *et al.* 2007). It is difficult to establish whether, and when, a period of fastest exhumation occurred on Tinos, especially because it is not clear where the ages of 24–21 Ma should be plotted along the greenschist facies segment of the pressure–temperature path. If, however, a closure temperature of about 500 °C is accepted for the Rb–Sr system in white mica (Bröcker & Franz 1998, 2005), then, using the path obtained by Parra *et al.* (2002), this age range should coincide with pressures around 6 kbar. Pressures associated with the thermal aureole of the *c*. 15 Ma-old Tinos intrusion are around 2–3 kbars (e.g. Bröcker & Franz 2000). Taken together, using a factor of 3.64 to convert pressures (kbar) into depths (km), these values yield a mean exhumation rate around 1.5–2 mm/a during the period from *c*. 22 to 15 Ma. The apatite fission track ages indicate that later exhumation was slower. If the earlier episode of heating at about 9 kbar ended at *c*. 30 Ma, as suggested by Parra *et al.* (2002) (see 'Post-orogenic versus syn-orogenic extension' section), then a mean exhumation rate around 1.4 mm/a is suggested for the period from *c*. 30 to 22 Ma. These estimates are crude, nevertheless they suggest that exhumation proceeded either at constant rate from *c*. 30 Ma to 15 Ma, or was a bit faster during the 22–15 Ma interval.

The cooling history of Syros is very poorly known. At least part of the displacement along the detachment seen in southeastern Syros occurred later than 30 Ma (see 'Interfering detachment systems' section). Zircon fission track ages are around 20 Ma in the hanging wall and around 11 Ma in the footwall, suggesting that the detachment was active at *c*. 11 Ma (Ring *et al.* 2003). All the footwall samples come from northern Syros, so that it is not clear whether the age gap of 9 Ma reflects displacement along the detachment itself or/and along one of the low-angle normal faults that dissect the footwall (Ridley 1984). Summing up, a sound comparison between Tinos and Syros is out of reach so far, nevertheless available radiometric data leave it possible that the Tinos MCC formed earlier.

The above review also indicates that the two island pairs (Naxos–Ios and Tinos–Syros) may have formed contemporaneously. The Naxos MCC experienced its fastest exhumation between *c*. 17 and 12 Ma, while the Tinos MCC may have done so between *c*. 22 and 15 Ma. Thus, the two MCCs could be broadly

coeval. In contrast, Jolivet *et al.* (2004) claimed that the Naxos MCC has formed *c*. 5 Ma later than the Tinos MCC has. They further proposed that, in the Cyclades, 'a-type' MCCs (domes with an axis parallel to extension, like on Naxos) are associated with greater exhumation and formed later than 'b-type' MCCs (domes with an axis perpendicular to extension, like on Tinos). This interpretation largely arises from the assumption that the main intrusion on Tinos emplaced as early as 20–19 Ma, as initially proposed by Altherr *et al.* (1982). As stated above, however, available radiometric data make it possible that the whole composite intrusion of Tinos emplaced at *c*. 15 Ma. We also notice that the Ios MCC is clearly a 'a-type' dome (e.g. Gautier & Brun 1994*a*; Vandenberg & Lister 1996), yet, at variance with the hypothesis of Jolivet *et al.* (2004), it did not exhume higher grade rocks than the Tinos MCC did, and recorded extensional shearing as early as *c*. 20.5 Ma (Baldwin & Lister 1998), that is, at the same time as on Tinos.

Implications for the conditions of extension in the Cyclades

Insofar as the numerical experiments presented in this study adequately simulate the process of lithospheric extension, their comparison with the case of the Cyclades suggests a relatively narrow range of conditions for the development of post-orogenic extension in the Central Aegean region during the late Cenozoic. We now review and discuss these conditions.

Conditions at the onset of post-orogenic extension. A first inference concerns the mean thickness of the crust at the onset of post-orogenic extension. The present crustal thickness of 25–26 km in the Cyclades suggests an initial thickness of *c*. 43–44 km (see 'Moho depth' section and Fig. 7e), in line with the range of *c*. 41–44 km suggested by the width of the Naxos and Paros first-generation MCCs (see 'Geometry of MCCs' section and Fig. 7a). These values are consistent with (rough) estimates in the literature (e.g. McKenzie 1978; Le Pichon & Angelier 1979; Gautier *et al.* 1999) and compare well with the current crustal thickness of $\leq$ 46km in the western Hellenides of mainland Greece (Makris 1975), where extension has played only a minor role.

A second inference concerns the thermal state of the lithosphere at the onset of extension. The numerical experiments suggest an initial thickness of the thermal lithosphere of only *c*. 60 km (corresponding to an initial Moho temperature of 1070 °C at 44 km). Measurements of the present heat flow in the Aegean (Jongsma 1974; Erickson *et al.* 1977; Makris & Stobbe 1984) document the presence of a hot lithosphere. Seismic surface-wave data are consistent with a lithosphere-asthenosphere boundary at a depth between 40 and 50 km (Endrun *et al.* 2008) and, thus, with a high thermal profile of the lithosphere at present. As for the thermal state of the Aegean lithosphere at the onset of post-orogenic extension, it may be deduced from the pressure-temperature path of metamorphic rocks involved in the MCCs.

Figure 10 displays the well-documented cases of Naxos (data from the migmatitic core of the MCC) and Tinos. In the latter case, only the second episode of exhumation is considered (cf. Parra *et al.* 2002) as this is the most likely to reflect post-orogenic extension (see 'Post-orogenic *vs*. syn-orogenic extension' section). Figure 10 also displays the geotherm associated with an experiment in which the thermal lithosphere is 60 km-thick. The figure shows that, for Naxos, the conditions at the temperature peak coincide with the numerical geotherm. For Tinos, the 'post-orogenic' exhumation path starts away from this geotherm and crosses it at conditions equivalent to a pressure of 5 kbar. Geochronological constraints (see sections 'Post-orogenic *vs*. syn-orogenic extension' and Timing of exhumation') suggest that this happens at about the same time (*c*. 21 Ma) as the attainment of peak temperatures on Naxos (Fig. 10). Therefore, at this time, Tinos and Naxos plot together along the numerical geotherm. On the one hand, this confirms that a lithosphere only *c*. 60 km-thick is a realistic condition at relatively early stages of post-orogenic extension in the Cyclades. On the other hand, the conditions at the onset of the second episode of exhumation on Tinos (550 °C at 9 kbar; Parra *et al.* 2002) imply a fairly low geothermal gradient (16.8 °C/km) and plot along a numerical geotherm corresponding to a 100 km-thick lithosphere (dashed line in Fig. 10). Insofar as the entire secondary exhumation on Tinos reflects post-orogenic extension, this indicates that the earliest stages of this extension occurred while the lithosphere was still thick. The exhumation paths of both Tinos and Naxos are consistent with the view that this lithosphere has been warmed up until the time it attained the conditions enabling the development of interfering MCCs (i.e. a *c*. 60 km-thick lithosphere), at *c*. 21 Ma. In any case, much of the post-orogenic extensional phase and, within it, the period of development of MCCs occurred while the lithosphere was thin and hot. This is shown by our numerical results and is also in line with several other numerical studies (Block & Royden 1990; Buck 1991; Tirel *et al.* 2004*a*, 2008; Rosenbaum *et al.* 2005; Wijns *et al.* 2005; Gessner *et al.* 2007). In Figure 10, latest stages of the exhumation paths suggest the existence of geotherms even higher than the one associated with a 60 km-thick lithosphere. This may reflect the

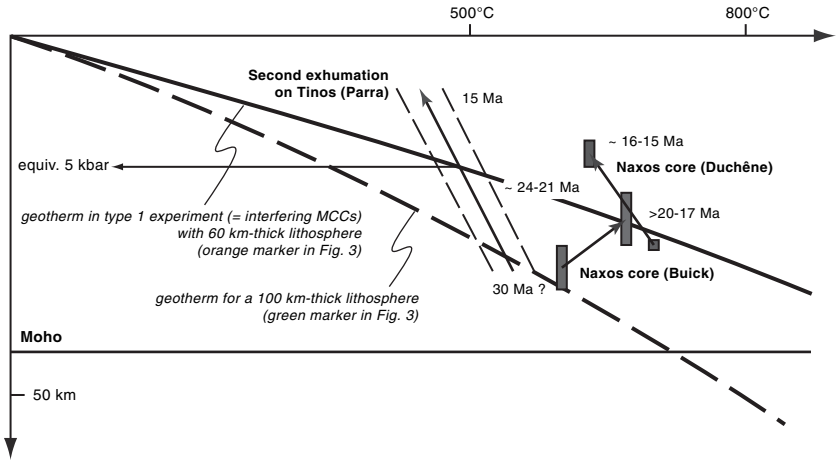

Fig. 10. Comparison between the geotherms associated with two numerical experiments and the exhumation path of metamorphic rocks on Tinos (after Parra *et al.* 2002) and Naxos (after Buick & Holland 1989 and Duchêne *et al.* 2006). A factor of 3.64 was used to convert pressures (kbar) into depths (km). Age constraints are discussed in sections 'Post-orogenic versus syn-orogenic extension' and 'Timing of exhumation'.

ongoing increase of the regional geothermal gradient or/and the local rise of isotherms during MCC development (see 'Geometry of MCCs' section and Gessner *et al.* 2007).

Recently, several studies have shown evidence for a high temperature regime in the shallow mantle and a thin lithosphere (1200 °C at a depth of *c.* 60 km) over widths of 250 to >900 km in several subduction zone back-arc domains unaffected by extensional processes (Currie *et al.* 2004; Hyndman *et al.* 2005; Currie & Hyndman 2006). The authors suggest that heat is rapidly carried upward by vigorous thermal convection in the upper mantle below the overriding plate. This small-scale convection could be promoted by the low viscosities associated with the addition of water, resulting in a reduction of the strength of the base of the lithosphere and its rapid 'erosion' (Arcay *et al.* 2005, 2006). The Cyclades area may have been affected by such processes prior to *c.* 21 Ma (i.e. while warming the lithosphere until its thickness was reduced to *c.* 60 km, cf. Fig. 10) provided it was already lying in the back-arc domain of the South Hellenic subduction zone at that time, which is a matter of debate (e.g. Ring & Layer 2003; Jolivet *et al.* 2004; Pe-Piper & Piper 2006).

Alternatively, the pioneering suggestion of Bird (1978) concerning continental mantle delamination as a cause of strong heating of the crust appears attractive. In the Aegean, this process was first suggested by Zeilinga de Boer (1989) and has been explicitely invoked in a number of recent studies (Thomson *et al.* 1999; Jolivet *et al.* 2003; Faccenna *et al.* 2003; Ring & Layer 2003). Support to this hypothesis is found in a recent review of the late Cenozoic magmatism of the Aegean by Pe-Piper & Piper (2006), as discussed below.

Boundary velocity during MCC-type extension in the Cyclades. In the experiments, the range of boundary velocities which succesfully led to a sequential development of interfering MCCs lies between 1 and 2.7 cm/a. In addition, the present crustal thickness of 25–26 km in the Cyclades suggests a velocity of *c.* 2.0–2.3 cm/a (see 'Moho depth' section and Fig. 7f), while the width of the Naxos and Paros first-generation MCCs (see 'Geometry of MCCs' section) and the duration of MCC-type extension in the Cyclades (see 'Timing of exhumation' section) seem to exclude values lower than *c.* 2 cm/a (Fig. 7b) and *c.* 1.7 cm/a (Fig. 7d), respectively. Hence, the experimental results predict a velocity at the boundary of the stretching domain around 2.0–2.3 cm/a, while lower values seem excluded.

In the case of the Cyclades, this velocity should correspond to the rate at which the South Hellenic subduction retreated during MCC-type extension. In addition, as MCC-type extension in the Cyclades lasted between about 12 and 24 Ma (from 30–23 to 11–6–Ma, see 'Timing of exhumation' section), the associated amount of retreat is predicted to lie between about 240 km (for 12 Ma at 2 cm/a) and 550 km (for 24 Ma at 2.3 cm/a).

These values can be compared with various estimates in the literature. For instance, Faccenna *et al.* (2003) have considered 250 km of retreat during the

period from 30 to 5 Ma, hence at a velocity of only 1 cm/a. In contrast, a retreat velocity as high as 3 cm/a has been proposed by Jolivet *et al.* (1998) on the basis of the southward migration of arc magmatism since *c*. 32 Ma (Fytikas *et al.* 1984), assuming the underlying slab kept a constant dip. However, the graph from which this value is deduced (Jolivet *et al.* 1998, Fig. 21b) actually yields a value of about 2.2 cm/a and considers 700 km of migration of arc magmatism, which exceeds by at least 100 km the actual value. Instead, considering about 550 km of migration of magmatism since about 32 Ma (see van Hinsbergen 2004 for a recent compilation) would yield a retreat velocity of 1.7 cm/a, in fair agreement with our numerical analysis. However, among the 550 km of migration, as much as 90 km may be considered as balanced, not by extensional strain but by the lateral extrusion of Anatolia during the last few million years (e.g. Gautier *et al.* 1999), which could lower the boundary velocity of the extensional system to 1.4 cm/a. It is also worth noting that the migration of magmatism is not an ideal mean for quantifying retreat, firstly because the assumption of a constant slab dip may not be valid, and secondly because not every magmatic rock may reflect arc magmatism. Pe-Piper & Piper (2006) recently argued that most Cenozoic magmatic rocks of the Aegean bear petrogeochemical characteristics that are not typical of arc processes and suggest instead that they reflect either slab break-off or delamination of the lithospheric mantle. At first sight, this seems to exclude the migration of magmatism as an appropriate tool to document subduction retreat. However, tomography images of the Aegean mantle are clearly more compatible with progressive delamination of a continuous slab (*sensu* Bird 1978) rather than break-off of several slabs (e.g. Faccenna *et al.* 2003; van Hinsbergen *et al.* 2005*a*). The dynamics of mantle delamination is broadly equivalent to that of a retreating subduction, therefore the migration of delamination-related magmatism may actually be appropriate to quantify retreat (e.g. Zeilinga de Boer 1989).

Another estimate of the amount of retreat may arise from a comparison between the initial and present shape of the Aegean frontal arc. For instance, Gautier *et al.* (1999) suggested a smoothly curved arc at the onset of Aegean extension, which led them to propose about 440 km of retreat (of which 90 km would be balanced by the lateral extrusion of Anatolia, leaving 350 km to be balanced by extensional strain). The end-member case leading to maximum retreat is probably that of an initially rectilinear arc. Using the same arc extremities as in Gautier *et al.* (1999), this case would yield about 600 km of retreat, in reasonable agreement with the value suggested by the migration of magmatism. This would yield about 510 km balanced by extensional strain. If we assume that retreat occurred essentially during MCC-type extension in the Cyclades, then the boundary velocity of the extensional system could have been as high as 2.1 cm/a if extension lasted 24 Ma (starting at *c*. 30 Ma), in good agreement with our numerical analysis, or as high as 4.2 cm/a if extension lasted 12 Ma (starting at *c*. 23 Ma). The latter value is clearly too high and suggests that MCC-type extension in the Cyclades started significantly before 23 Ma or/and that the total amount of retreat has been significantly less than in the above end-member case, or/and that a significant part of the retreat occurred before or/and after MCC-type extension in the Cyclades.

Conclusions

Our numerical analysis suggests that, for certain conditions, MCCs may interfere and develop in sequence during continental extension. Like common claims in the literature, we find that 'inward' flow of an extremely weak lower crust is required for MCCs to develop, while a sub-Moho mantle of very low strength appears to be another necessary condition for maintaining the Moho flat. As a result of lower crustal inward flow, two conjugate flat-lying shear zones form during the early development of the first MCC, one of which later evolves as a typical detachment. In the experiments with interfering MCCs, the second MCC starts to develop right above one of the previously formed shear zones. This shear zone is dragged upward during dome amplification and, due to renewed inward flow, is reactivated with the same kinematics along one dome limb and with the opposite kinematics along the other dome limb.

The Cyclades archipelago is characterized by three closely spaced chains of MCCs developed largely during Miocene extension. We found that the geometry and kinematic pattern of adjacent MCCs along the Naxos–Ios and the Tinos–Syros transects compare well with the numerical experiments. Available geochronological data for these islands are not detailed enough to document a sequential development of MCCs, nevertheless they remain compatible with this hypothesis. We also compared features of the numerical experiments, such as the final Moho depth, the duration of MCC-type extension, and the width of the domes at the end of the exhumation process, to equivalent features in the Cyclades in order to tentatively constrain the initial and boundary conditions suitable to the Aegean case. This comparison leads us to infer a crustal thickness in the range of 40 to 44 km in the Cyclades at the onset of post-orogenic extension. A thermal lithospheric thickness of only

c. 60 km is also inferred, which might be a condition at the onset of extension or may have been obtained during early stages of extension while the lithosphere was warmed up. Either a backarc subduction setting or a process of mantle delamination may account for this situation.

The experiments also suggest a boundary velocity of 2.0–2.3 cm/a, which should basically reflect the rate at which the South Hellenic subduction zone retreated. Considering *c*. 500 km as an upper bound for the amount of retreat balanced by Aegean extension, and assuming that this retreat mostly occurred during MCC-type extension, in the Cyclades, the boundary velocity could have been as high as 2.1 cm/a (if MCC-type extension lasted 24 Ma, starting at *c*. 30 Ma and finishing at *c*. 6 Ma): this is in good agreement with the numerical analysis.

The post-doctoral grant of C.T. and computational resources were funded by ISES (Netherlands Research Centre for Integrated Solid Earth Science). C.T. thanks E. Burov, Y. Podladchikov and A. Poliakov who have co-developed the kernel of PARAVOZ. D. J. J. v. H. is funded through an NWO-VENI grant. We thank R. Govers, J.-P. Brun and E. Burov for discussions at various stages of the project. We gratefully acknowledge the editor, M. Edwards, and the two reviewers S. Buiter and M. Bröcker for their thoughtful reviews that improved our manuscript.

References

ALTHERR, R., KREUZER, H., WENDT, I., LENZ, H., WAGNER, G. A., KELLER, J., HARRE, W. & HÖHNDORF, A. 1982. A Late Oligocene/Early Miocene high temperature belt in the Attic-Cycladic crystalline complex (SE Pelagonian, Greece). *Geologisches Jahrbuch*, **E23**, 97–164.

ALTHERR, R., SCHLIESTEDT, M., OKRUSCH, M., SEIDEL, E., KREUZER, H., HARRE, W., LENZ, H., WENDT, I. & WAGNER, G. A. 1979. Geochronology of High-Pressure Rocks on Sifnos (Cyclades, Greece). *Contributions to Mineralogy and Petrology*, **70**, 245–255.

ANDRIESSEN, P. A. M. 1991. K-Ar and Rb-Sr age determinations on micas of impure marbles of Naxos, Greece: the influence of metamorphic fluids and lithology on the blocking temperature. *Schweizerische Mineralogische and Petrographische Mitteilungen*, **71**, 89–99.

ANDRIESSEN, P. A. M., BOELRIJK, N. A. I. M., HEBEDA, E. H., PRIEM, H. N. A., VERDURMEN, E. A. T. & VERSCHURE, R. H. 1979. Dating the events of metamorphism and granitic magmatism in the Alpine Orogen of Naxos (Cyclades, Greece). *Contributions to Mineralogy and Petrology*, **69**, 215–225.

ANGELIER, J. 1977*a*. Sur l'évolution tectonique depuis le Miocène supérieur d'un arc insulaire méditerranéen: l'arc égéen. *Revue de Géographie physique et Géologie dynamique*, **XIX**, 271–294.

ANGELIER, J. 1977*b*. Essai sur la néotectonique et les derniers stades tarditectoniques de l'arc égéen et de l'Egée méridionale. *Bulletin de la Societé Géologique de France*, **XIX**, 651–662.

ANGELIER, J., GLACON, G. & MULLER, C. 1978. Sur la présence et la position tectonique du Miocène inférieur marin dans l'archipel de Naxos (Cyclades, Grèce). *Comptes Rendus de l'Académie des Sciences de Paris*, **286**, 21–24.

ARCAY, D., TRIC, E. & DOIN, M.-P. 2005. Numerical simulations of subduction zones. Effect of slab deshydration on the mantle wedge dynamics. *Physics of the Earth and Planetary Interiors*, **149**, 133–153.

ARCAY, D., DOIN, M.-P., TRIC, E., BOUSQUET, R. & DE CAPITANI, C. 2006. Overriding plate thinning in subduction zones: Localized convection induced by slab deshydration. *Geochemistry Geophysics Geosystems*, **7**, doi:10.1029/2005GC0011061.

AVIGAD, D. 1993. Tectonic juxtaposition of blueschists and greenschists in Sifnos Islands (Aegean Sea)—implications for the structure of the Cycladic blueschist belt. *Journal of Structural Geology*, **15**, 1459–1469.

AVIGAD, D. & GARFUNKEL, Z. 1989. Low angle faults above and below a blueschist belt—Tinos Island, Cyclades, Greece. *Terra Nova*, **1**, 182–187.

AVIGAD, D., GARFUNKEL, Z., JOLIVET, L. & AZAÑON, J. M. 1997. Backarc extension and denudation of Mediterranean eclogites. *Tectonics*, **16**, 924–941.

AVIGAD, D., BAER, G. & HEIMANN, A. 1998. Block rotations and continental extension in the central Aegean Sea: palaeomagnetic and structural evidence from Tinos and Mykonos (Cyclades, Greece). *Earth and Planetary Science Letters*, **157**, 23–40.

AVIGAD, D., ZIV, A. & GARFUNKEL, Z. 2001. Ductile and brittle shortening, extension-parallel folds and maintenance of crustal thickness in the central Aegean (Cyclades, Greece). *Tectonics*, **20**, 277–287.

BALDWIN, S. L. & LISTER, G. S. 1998. Thermochonology of the South Cyclades Shear Zone, Ios, Greece: Effects of ductile shear in the argon partial retention zone. *Journal of Geophysical Research*, **103**, 7315–7336.

BIRD, P. 1978. Initiation of intracontinental subduction in the Himalaya. *Journal of Geophysical Research*, **83**, 4975–4987.

BLOCK, L. & ROYDEN, L. H. 1990. Core complex geometries and regional scale flow in the lower crust. *Tectonics*, **9**, 557–567.

BOND, C. E., BUTLER, R. W. H. & DIXON, J. E. 2007. Co-axial horizontal stretching within extending orogens: the exhumation of HP rocks on Syros (Cyclades) revisited. *In*: RIES, A. C., BUTLER, R. W. H. & GRAHAM, R. H. (eds) *Deformation of the Continental Crust: The Legacy of Mike Coward*. Geological Society, London, Special Publication, **272**, 203–222.

BONNEAU, M. 1982. Evolution géodynamique de l'arc égéen depuis le Jurassique supérieur jusqu'au Miocène. *Bulletin de la Societé Géologique de France*, **XXIV**, 229–242.

BOZKURT, E. 2001. Late Alpine evolution of the central Menderes Massif, western Turkey. *International Journal of Earth Sciences*, **89**, 728–744.

BRICHAU, S., RING, U., KETCHAM, R. A., CARTER, A., STOCKLI, D. & BRUNEL, M. 2006. Constraining the long-term evolution of the slip rate for a major extensional fault system in the central Aegean, Greece, using thermochronology. *Earth and Planetary Science Letters*, **241**, 293–306.

BRICHAU, S., RING, U., CARTER, A., MONIÉ, P., BOLHAR, R., STOCKLI, D. & BRUNEL, M. 2007. Extensional faulting on Tinos Island, Aegean Sea, Greece: How many detachments? *Tectonics*, **26**, TC4009, doi:10.1029/2006TC001969.

BRÖCKER, M. 1990. Blueschist-to-greenschist transition in metabasites from Tinos Island (Cyclades, Greece): Compositional control or fluid infiltration? *Lithos*, **25**, 25–39.

BRÖCKER, M. & FRANZ, L. 1998. Rb–Sr isotope studies on Tinos Island (Cyclades, Greece): additional time constraints for metamorphism, extent of infiltration-controlled overprinting and deformational activity. *Geological Magazine*, **135**, 369–382.

BRÖCKER, M. & FRANZ, L. 2000. The contact aureole on Tinos (Cyclades, Greece): tourmaline-biotite geothermometry and Rb-Sr geochronology. *Mineralogy and Petrology*, **70**, 257–283.

BRÖCKER, M. & FRANZ, L. 2005. The base of the Cycladic blueschist unit on Tinos Island (Greece) re-visited: Field relationships, phengite chemistry and Rb–Sr geochronology. *Neues Jahrbuch für Mineralogie, Abhandlungen*, **181**, 81–93.

BRÖCKER, M. & FRANZ, L. 2006. Dating metamorphism and tectonic juxtaposition on Andros Island (Cyclades, Greece): results of a Rb–Sr study. *Geological Magazine*, **143**, 1–12.

BRÖCKER, M., BIELING, D., HACKER, B. & GANS, P. B. 2004. High-Si phengite records the time of greenschist facies overprinting: implications for models suggesting mega-detachments in the Aegean Sea. *Journal of Metamorphic Geology*, **22**, 427–442.

BRUN, J.-P., SOKOUTIS, D. & VAN DEN DRIESSCHE, J. 1994. Analogue modeling of detachment fault systems and core complexes. *Geology*, **22**, 319–322.

BRUN, J.-P. & VAN DEN DRIESSCHE, J. 1994. Extensional gneiss domes and detachment fault systems; structure and kinematics. *Bulletin de la Societé Géologique de France*, **165**, 519–530.

BUCK, W. R. 1991. Modes of continental lithospheric extension. *Journal of Geophysical Research*, **96**, 20161–20178.

BUICK, I. S. 1991. The late Alpine evolution of an extensional shear zone, Naxos, Greece. *Journal of the Geological Society of London*, **148**, 93–103.

BUICK, I. S. & HOLLAND, T. J. B. 1989. The P-T-t path associated with crustal extension, Naxos, Cyclades, Greece. *In*: DALY, J. S., CLIFF, R. A. & YARDLEY, B. W. D. (eds) *Evolution of Metamorphic Belts*. Geological Society, London, Special Publication, **43**, 365–369.

BURG, J. P., VAN DEN DRIESSCHE, J. & BRUN, J.-P. 1994. Syn to post-thickening extension in the Variscan Belt of Western Europe: Modes and structural consequences. *Géologie de la France*, **3**, 33–51.

BUROV, E. & CLOETINGH, S. 1997. Erosion and rift dynamics; new thermomechanical aspects of post-rift evolution of extensional basins. *Earth and Planetary Science Letters*, **150**, 7–26.

BUROV, E. B. & GUILLOU-FROTTIER, L. 1999. Thermomechanical behavior of large ash flow calderas. *Journal of Geophysical Research*, **104**, 23081–23109.

BUROV, E. & POLIAKOV, A. 2001. Erosion and rheology controls on synrift and postrift evolution; verifying old and new ideas using a fully coupled numerical model. *Journal of Geophysical Research*, **106**, 16461–16481.

BUROV, E. & POLIAKOV, A. N. B. 2003. Erosional forcing on basin dynamics: new aspects of syn- and post-rift evolution. *In*: NIEUWLAND, D. A. (ed.) *New Insights into Structural Interpretation and Modelling*. Geological Society, London, Special Publication, **212**, 209–224.

BUROV, E. & GUILLOU-FROTTIER, L. 2005. The plume head-continental lithosphere interaction using a tectonically realistic formulation for the lithosphere. *Geophysical Journal International*, **161**, 469–490.

BUROV, E. B., JAUPART, C. & GUILLOU-FROTTIER, L. 2003. Ascent and emplacement of buoyant magma bodies in brittle–ductile upper crust. *Journal of Geophysical Research*, **108**, 2177–2189.

BYERLEE, J. D. 1978. Friction of rocks. *Pure and Applied Geophysics*, **116**, 615–626.

CHÉRY, J. 2001. Core complex mechanics: From the Gulf of Corinth to the Snake Range. *Geology*, **29**, 439–442.

CONEY, P. J. 1980. Cordilleran metamorphic core complexes: an overview. *In*: CRITTENDEN, M. C., CONEY, P. J. & DAVIS, G. H. (eds) *Cordilleran Metamorphic Core Complexes*. Geological Society of America Memoir, **153**, 7–31.

CUNDALL, P. A. 1989. Numerical experiments on localization in frictional materials. *Ingenieur-Archiv*, **59**, 148–159.

CURRIE, C. A. & HYNDMAN, R. D. 2006. The thermal structure of subduction zone back arcs. *Journal of Geophysical Research*, **111**, B08404, doi:10.1029/2005JB004024.

CURRIE, C. A., WANG, K., HYNDMAN, R. D. & HE, J. 2004. The thermal effects of steady-state slab-driven mantle flow above a subducting plate: the Cascadia subduction zone and backarc. *Earth and Planetary Science Letters*, **223**, 35–48.

DAVIS, G. H. 1980. Structural characteristics of metamorphic core complexes, southern Arizona. *In*: CRITTENDEN, M. C., CONEY, P. J. & DAVIS, G. H. (eds) *Cordilleran Metamorphic Core Complexes*. Geological Society of America Memoir, **153**, 35–77.

DUBOIS, R. & BIGNOT, G. 1979. Présence d'un 'hard ground' nummulitique au sommet de la série cretacée d'Almyropotamos (Eubée méridionale, Grèce). *Comptes Rendus de l'Académie des Sciences de Paris*, **289**, 993–995.

DUCHÊNE, S., AÏSSA, R. & VANDERHAEGHE, O. 2006. Pressure-Temperature-time evolution of metamorphic rocks from Naxos (Cyclades, Greece): constraints from thermobarometry and Rb/Sr dating. *Geodinamica Acta*, **19**, 301–321.

ENDRUN, B., MEIER, T., LEBEDEV, S., BOHNHOFF, M., STAVRAKAKIS, G. & HARJES, H.-P. 2008. *S* velocity structure and radial anisotropy in the Aegean region

from surface wave dispersion. *Geophysical Journal International*, **174**, 593–616.

ERICKSON, A. J., SIMMONS, G. & RYAN, W. B. F. 1977. Review of heatflow data from the Mediterranean and Aegean Seas. *In*: BIJU-DUVAL, B. & MONTADERT, L. (eds) *International Symposium on the Structural History of the Mediterranean Basins, Split, Yugoslavia*. Technip, Paris, 263–279.

FACCENNA, C., JOLIVET, L., PIROMALLO, C. & MORELLI, A. 2003. Subduction and the depth of convection of the Mediterranean mantle. *Journal of Geophysical Research*, **108**(B2), 2099, doi:10.1029/2001JB001690.

FORSTER, M. A. & LISTER, G. S. 1999. Detachment faults in the Aegean Core Complex of Ios, Greece. *In*: RING, U., BRANDON, M. T., LISTER, G. S. & WILLETT, S. D. (eds) *Exhumation Processes: Normal Faulting, Ductile Flow and Erosion*. Geological Society, London, Special Publication, **154**, 305–323.

FYTIKAS, M., INNOCENTI, F., MANETTI, P., MAZZUOLI, R., PECCERILLO, A. & VILLARI, L. 1984. Tertiary to Quarternary evolution of volcanism in the Aegean region. *In*: DIXON, J. E. & ROBERTSON, A. H. F. (eds) *The Geological Evolution of the Eastern Mediterranean*. Geological Society, London, Special Publication, **17**, 687–699.

GANOR, J., MATTHEWS, A., SCHLIESTEDT, M. & GARFUNKEL, Z. 1996. Oxygen isotopic heterogeneities of metamorphic rocks: an original tectonostratigraphic signature or an imprint of exotic fluids? A case of study of Sifnos and Tinos islands (Greece). *European Journal of Mineralogy*, **8**, 719–732.

GAUTIER, P. 1995. *Géométrie crustale et cinématique de l'extension tardi-orogénique dans le domaine centre-égéen (îles des Cyclades et d'Eubée, Grèce)*. PhD Thesis, University of Rennes 1, France. Mémoires Géosciences Rennes, **61**, 1–417.

GAUTIER, P. 2000. Comment to "Back-arc extension and denudation of Mediterranean eclogites". *Tectonics*, **19**, 406–409.

GAUTIER, P. & BRUN, J.-P. 1994*a*. Ductile crust exhumation and extensional detachments in the central Aegean (Cyclades and Evvia islands). *Geodinamica Acta*, **7**, 57–85.

GAUTIER, P. & BRUN, J.-P. 1994*b*. Crustal-scale geometry and kinematics of late-orogenic extension in the central Aegean (Cyclades and Evvia Island). *Tectonophysics*, **238**, 399–424.

GAUTIER, P., BRUN, J.-P. & JOLIVET, L. 1993. Structure and kinematics of Upper Cenozoic extensional detachment on Naxos and Paros (Cyclades Islands, Greece). *Tectonics*, **12**, 1180–1194.

GAUTIER, P., BRUN, J.-P., MORICEAU, R., SOKOUTIS, D., MARTINOD, J. & JOLIVET, L. 1999. Timing, kinematics and cause of Aegean extension: a scenario based on a comparison with simple analogue experiments. *Tectonophysics*, **315**, 31–72.

GERBAULT, M., BUROV, E. B., POLIAKOV, A. N. B. & DAGNIÈRES, M. 1999. Do faults trigger folding in the lithosphere? *Geophysical Research Letters*, **26**, 271–274.

GESSNER, K., RING, U., JOHNSON, C., HETZEL, R., PASSCHIER, C. W. & GÜNGÖR, T. 2001. An active bivergent rolling-hinge detachment system: Central Menderes metamorphic core complex in western Turkey. *Geology*, **29**, 611–614.

GESSNER, K., WIJNS, C. & MORESI, L. 2007. Significance of strain localization in the lower crust for structural evolution and thermal history of metamorphic core complexes. *Tectonics*, **26**, TC2012, doi:10.1029/2004TC001768.

GRASEMANN, B., EDWARDS, M. A., IGLSEDER, C., PETRAKAKIS, K., SCHNEIDER, D. & Accel Team. 2007. Tertiary SSW directed crustal extension in the Western Cyclades: A new kinematic domain in the Aegean region (Greece). *Geophysical Research Abstracts*, **9**, SRef-ID: 1607-7962/gra/EGU2007-A-06656.

GOETZE, C. 1978. The mechanisms of creep olivine. *Philosophical Transactions of the Royal Society of London*, **A288**, 99–119.

GUEYDAN, F., LEROY, Y. M. & JOLIVET, L. 2004. Mechanics of low-angle shear zones at the brittle-ductile transition. *Journal of Geophysical Research*, **109**, B12407, doi:10.1029/2003JB002806.

HANDY, M. 1989. Deformation regimes and the rheological evolution of fault zones in the lithosphere: the effects of pressure, temperature, grain size, and time. *Tectonophysics*, **163**, 119–152.

HANSEN, F. D. & CARTER, N. L. 1982. Creep of Selected Crustal Rocks at 1000 MPa. *Eos, Transactions, American Geophysical Union*, **63**, 437.

HAUSER, E., POTTER, C., HAUGE, T., BURGESS, S., BURTCH, S., MURTSCHLER, J. *ET AL*. 1987. Crustal structure of eastern Nevada from COCORP deep seismic reflection data. *Geological Society of American Bulletin*, **99**, 833–844.

HEJL, E., RIEDL, H., SOULAKELLIS, N., VAN DEN HAUTE, P. & WEINGARTNER, H. 2003. Fission-track dating of the south-eastern Bohemian Massif (Waldviertel, Austria); thermochronology and long-term erosionYoung Neogene tectonics and relief development on the Aegean islands of Naxos, Paros and Ios (Cyclades, Greece). *Mitteilungen der Österreichischen Geologischen Gesellschaft*, **93**, 105–127.

HEJL, E., RIEDL, H. & WEINGARTNER, H. 2002. Post-plutonic unroofing and morphogenesis of the Attic-Cycladic complex (Aegea, Greece). *Tectonophysics*, **349**, 37–56.

HENJES-KUNST, F. & KREUZER, H. 1982. Isotopic dating of pre-alpidic rocks from the island of Ios (Cyclades, Greece). *Contributions to Mineralogy and Petrology*, **80**, 245–253.

HYNDMAN, R. D., CURRIE, C. A. & MAZZOTTI, S. P. 2005. Subduction zone backarcs, mobile belts, and orogenic heat. *GSA Today*, **15**, 4–10.

IGLSEDER, C., GRASEMANN, B., PETRAKAKIS, K., EDWARDS, M. A., ZAMOLYI, A., RAMBOUSEK, C., HÖRFARTER, C. *ET AL*. 2006. Multistage Plutonism and the Serifos Detachment System (Cyclades, Greece). *Geophysical Research Abstracts*, **8**, SRef-ID: 1607–7962/gra/EGU06-A-05118.

JOLIVET, L. & PATRIAT, M. 1999. Ductile extension and the formation of the Aegean Sea. *In*: DURAND, B., JOLIVET, L., HORVATH, F. & SÉRANNE, M. (eds) *The Mediterranean Basins: Tertiary Extension within*

the Alpine Orogen. Geological Society, London, Special Publication, **156**, 427–456.

JOLIVET, L., FACCENNA, C., GOFFÉ, B., MATTEI, M., ROSSETTI, F., BRUNET, C. *ET AL.* 1998. Midcrustal shear zones in postorogenic extension: Example from the northern Tyrrhenian Sea. *Journal of Geophysical Research*, **103**, 12123–12160.

JOLIVET, L., FACCENNA, C., GOFFÉ, B., BUROV, E. & AGARD, P. 2003. Subduction tectonics and exhumation of high-pressure metamorphic rocks in the Mediterranean orogens. *American Journal of Science*, **303**, 353–409.

JOLIVET, L., FAMIN, V., MEHL, C., PARRA, T., AUBOURG, C., HÉBERT, R. & PHILIPPOT, P. 2004. Strain localization during crustal-scale boudinage to form extensional metamorphic domes in the Aegean Sea. *In*: WHITNEY, D. L., TEYSSIER, C. & SIDDOWAY, C. S. (eds) *Gneiss Domes in Orogeny*. Geological Society of America Special Paper, **380**, 185–210.

JONGSMA, D. 1974. Heat flow in the Aegean Sea. *Geophysical Journal of the Royal Astronomical Society*, **37**, 337–346.

KEAY, S., LISTER, G. S. & BUICK, I. 2001. The timing of partial melting, Barrovian metamorphism and granite intrusion in the Naxos metamorphic core complex, Cyclades, Aegean Sea, Greece. *Tectonophysics*, **342**, 275–312.

KIRBY, S. H. & KRONENBERG, A. K. 1987. Rheology of the Lithosphere: Selected Topics. *Reviews of Geophysics*, **25**, 1219–1244.

KIRSCHNER, D. L., COSCA, M. A., MASSON, H. & HUNZIKER, J. C. 1996. Staircase $^{40}Ar/^{39}Ar$ spectra of fine-grained white mica: Timing and duration of deformation and empirical constraints on argon diffusion. *Geology*, **24**, 747–750.

KUMERICS, C., RING, U., BRICHAU, S., GLODNY, J. & MONIÉ, P. 2005. The extensional Messaria shear zone and associated brittle detachment faults, Aegean sea, Greece. *Journal of the Geological Society of London*, **162**, 701–721.

LE PICHON, X. & ANGELIER, J. 1979. The Hellenic arc and trench system: a key to the neotectonic evolution of the eastern Mediterranean area. *Tectonophysics*, **60**, 1–42.

LE POURHIET, L., BUROV, E. & MORETTI, I. 2004. Rifting through a stack of inhomogeneous thrusts (the dipping pie concept). *Tectonics*, **23**, TC4005, doi:10.1029/2003TC001584.

LI, X., BOCK, G., VAFIDIS, A., KIND, R., HARJES, H.-P., HANKA, W. *ET AL.* 2003. Receiver function study of the Hellenic subduction zone: imaging crustal thickness variations and the oceanic Moho of the descending African lithosphere. *Geophysical Journal International*, **155**, 733–748.

LISTER, G. S., BANGA, G. & FEENSTRA, A. 1984. Metamorphic core complexes of Cordilleran type in the Cyclades, Aegean Sea, Greece. *Geology*, **12**, 221–225.

LOURENS, L. J., HILGEN, F. J., LASKAR, J., SHACKLETON, N. J. & WILSON, D. 2004. The Neogene period. *In*: GRADSTEIN, F. M., OGG, J. G. & SMITH, A. G. (eds) *A Geologic Time Scale 2004*. Cambridge University Press.

MAKRIS, J. 1975. Crustal structure of the Aegean Sea and the Hellenides obtained from geophysical surveys. *Journal of Geophysics*, **41**, 441–443.

MAKRIS, J. 1978. The crust and upper mantle of the Aegean region from deep seismic soundings. *Tectonophysics*, **46**, 269–284.

MAKRIS, J. & STOBBE, C. 1984. Physical properties and state of the crust and upper mantle of the eastern Mediterranean Sea deduced from geophysical data. *Marine Geology*, **55**, 347–363.

MAKRIS, J. & VEES, R. 1977. Crustal structure of the Central Aegan Sea and the islands of Evia and Crete, Greece, obtained by refractional seismic experiments. *Journal of Geophysics*, **42**, 329–341.

MALUSKI, H., BONNEAU, M. & KIENAST, J. R. 1987. Dating the metamorphic events in the Cycladic area: $^{39}Ar/^{40}Ar$ data from metamorphic rocks of the island of Syros (Greece). *Bulletin de la Societé Géologique de France*, **3**, 833–842.

MCCARTHY, J. & THOMPSON, G. A. 1988. Seismic imaging of extended crust with emphasis on the western United States. *Geological Society of America Bulletin*, **100**, 1361–1374.

MCKENZIE, D. 1978. Active tectonics of the Alpine-Himalayan belt: the Aegean Sea and surrounding regions. *Geophysical Journal of the Royal Astronomical Society*, **55**, 217–254.

MCKENZIE, D., NIMMO, F., JACKSON, J. A., GANS, P. B. & MILLER, E. L. 2000. Characteristics and consequences of flow in the lower crust. *Journal of Geophysical Research*, **105**, 11029–11046.

MEHL, C., JOLIVET, L. & LACOMBE, O. 2005. From ductile to brittle: evolution and localization of deformation below a crustal detachment (Tinos, Cyclades, Greece). *Tectonics*, **24**, TC4017, doi:10.1029/2004TC001767.

MORRIS, A. & ANDERSON, M. 1996. First paleomagnetic results from the Cycladic Massif, Greece, and their implications for Miocene extension directions and tectonic models in the Aegean. *Earth and Planetary Science Letters*, **142**, 397–408.

MÜLLER, M., GRASEMANN, B., EDWARDS, M. A., VOIT, K., IGLSEDER, C., ZAMOLYI, A. *ET AL.* 2006. Ductile to brittle progressive deformation within crustal-scale shear zones, Western Cyclades, Greece. *Geophysical Research Abstracts*, **8**, SRef-ID: 1607–7962/gra/EGU06-A-06943.

PARRA, T., VIDAL, O. & JOLIVET, L. 2002. Relation between the intensity of deformation and retrogression in blueschist metapelites of Tinos Island (Greece) evidenced by chlorite-mica local equilibria. *Lithos*, **63**, 41–66.

PARRISH, R. R., CARR, S. D. & PARKINSON, D. L. 1988. Eocene extensional tectonics and geochronology of the southern Omineca Belt, British Columbia and Washington. *Tectonics*, **7**, 181–212.

PATZAK, M., OKRUSCH, M. & KREUZER, H. 1994. The Akrotiri unit on the island of Tinos, Cyclades, Greece: Witness to a lost terrane of Late Cretaceous age. *Neues Jahrbuch für Geologie und Paläontologie Abhandlungen*, **194**, 211–252.

PE-PIPER, G. & PIPER, D. J. W. 2006. Unique features of the Cenozoic igneous rocks of Greece. *In*: DILEK, Y. & PAVLIDES, S. (eds) *Postcollisional tectonics and*

magmatism in the Mediterranean region and Asia. Geological Society of America Special Paper, **409**, 259–282.

POLIAKOV, A. N. B., PODLADCHIKOV, Y. & TALBOT, C. 1993. Initiation of salt diapirs with frictional overburdens: numerical experiments. *Tectonophysics*, **228**, 199–210.

RANALLI, G. 1987. *Rheology of the Earth*. Allen and Unwin, Boston.

REYNOLDS, S. J. & LISTER, G. S. 1990. Folding of mylonitic zones in Cordilleran metamorphic core complexes: evidences from near the mylonitic front. *Geology*, **18**, 216–219.

RIDLEY, J. 1984. Listric normal faulting and the reconstruction of the synmetamorphic structural pile of the Cyclades. *In*: DIXON, J. E. & ROBERTSON, A. H. F. (eds) *The Geological Evolution of the Eastern Mediterranean*. Geological Society of London Special Publication, **17**, 755–761.

RING, U. & LAYER, P. W. 2003. High-pressure metamorphism in the Aegean, eastern Mediterranean: Underplating and exhumation from the Late Cretaceous until the Miocene to Recent above the retreating Hellenic subduction zone. *Tectonics*, **22(3)**, 1022, doi:10.1029/2001TC001350.

RING, U. & REISCHMANN, T. 2002. The weak and superfast Cretan detachment, Greece: exhumation at subduction rates in extruding wedges. *Journal of the Geological Society of London*, **159**, 225–228.

RING, U., LAYER, P. W. & REISCHMANN, T. 2001. Miocene high-pressure metamorphism in the Cyclades and Crete, Aegean Sea, Greece: Evidence for large-magnitude displacement on the Cretan detachment. *Geology*, **29**, 395–398.

RING, U., GLODNY, J., WILL, T. & THOMSON, S. N. 2007*a*. An Oligocene extrusion wedge of blueschist-facies nappes on Evia, Aegean Sea, Greece: implications for the early exhumation of high-pressure rocks. *Journal of the Geological Society of London*, **164**, 637–652.

RING, U., WILL, T., GLODNY, J., KUMERICS, C., GESSNER, K., THOMSON, S. N. *ET AL*. 2007*b*. Early exhumation of high-pressure rocks in extrusion wedges: The Cycladic blueschist unit in the eastern Aegean, Greece and Turkey. *Tectonics*, **26**, TC2001, doi:10.1029/2005TC001872.

ROESLER, G. 1978. Relics of non-metamorphic sediments on central Aegean islands. *In*: CLOSS, H., ROEDER, D. & SCHMIDT, K. (eds) *Alps, Apennines, Hellenides*. Inter-Union Commission on Geodynamics Scientific Report, **38**, 480–481.

ROSENBAUM, G., AVIGAD, D. & SANCHEZ-GOMEZ, M. 2002. Coaxial flattening at deep levels of orogenic belts: evidence from blueschists and eclogites on Syros and Sifnos (Cyclades, Greece). *Journal of Structural Geology*, **24**, 1451–1462.

ROSENBAUM, G., REGENAUER-LIEB, K. & WEINBERG, R. 2005. Continental extension: From core complexes to rigid block faulting. *Geology*, **33**, 609–612. doi: 10.1130/G21477.1.

SACHPAZI, M., HIRN, A., NERCESSIAN, A., AVEDIK, F., MC BRIDE, J., LOUCOYANNAKIS, M. *ET AL*. 1997. A first coincident normal-incidence and wide-angle approach to studying the extending Aegean crust. *Tectonophysics*, **270**, 301–312.

SÁNCHEZ-GÓMEZ, M., AVIGAD, D. & HEIMANN, A. 2002. Geochronology of clasts in allochthonous Miocene sedimentary sequences on Mykonos and Paros Islands: implications for back-arc extension in the Aegean Sea. *Journal of the Geological Society of London*, **159**, 45–60.

SCHLIESTEDT, M. & MATTHEWS, A. 1987. Transformation of blueschist to greenschist facies rocks as a consequence of fluid infiltration, Sifnos (Cyclades), Greece. *Contributions to Mineralogy and Petrology*, **97**, 237–250.

THOMSON, S. N. & RING, U. 2006. Thermochronologic evaluation of post-collision extension in the Anatolide orogen, western Turkey. *Tectonics*, **25**, TC3005, doi:10.1029/2005TC001833.

THOMSON, S. N., STÖCKHERT, B. & BRIX, M. R. 1999. Miocene high-pressure metamorphic rocks of Crete, Greece: rapid exhumation by buoyant escape. *In*: RING, U., BRANDON, M. T., LISTER, G. S. & WILLETT, S. D. (eds) *Exhumation processes: Normal Faulting, Ductile Flow and Erosion*. Geological Society, London, Special Publication, **154**, 87–107.

TIREL, C., BRUN, J.-P. & BUROV, E. 2004*a*. Thermomechanical modeling of extensional gneiss domes. *In*: WHITNEY, D. L., TEYSSIER, C. & SIDDOWAY, C. S. (eds) *Gneiss Domes in Orogeny*. Geological Society of America Special Paper, **380**, 67–78.

TIREL, C., GUEYDAN, F., TIBERI, C. & BRUN, J.-P. 2004*b*. Aegean crustal thickness inferred from gravity inversion. Geodynamical implications. *Earth and Planetary Science Letters*, **228**, 267–280.

TIREL, C., BRUN, J.-P. & SOKOUTIS, D. 2006. Extension of thickened and hot lithospheres: Inferences from laboratory modeling. *Tectonics*, **25**, TC1005, doi:10.1029/2005TC001804.

TIREL, C., BRUN, J.-P. & BUROV, E. 2008. Dynamics and structural development of metamorphic core complexes. *Journal of Geophysical Research*, B04403, doi:10.1029/2005JB003694.

TROTET, F., JOLIVET, L. & VIDAL, O. 2001*a*. Tectono-metamorphic evolution of Syros and Sifnos islands (Cyclades, Greece). *Tectonophysics*, **338**, 179–206.

TROTET, F., VIDAL, O. & JOLIVET, L. 2001*b*. Exhumation of Syros and Sifnos metamorphic rocks (Cyclades, Greece). New constraints on the P-T paths. *European Journal of Mineralogy*, **13**, 901–920.

TURCOTTE, D. L. & SCHUBERT, G. 2002. *Geodynamics*. (2nd ed.) Cambridge University Press, Cambridge.

URAI, J. L., SCHUILING, R. D. & JANSEN, J. B. H. 1990. Alpine deformation on Naxos (Greece). *In*: KNIPE, R. J. & RUTTER, E. H. (eds) *Deformation Mechanisms, Rheology and Tectonics*. Geological Society, London, Special Publication, **54**, 509–522.

VAN DER MAAR, P. A. & JANSEN, J. B. H. 1983. The geology of the polymetamorphic complex of Ios, Cyclades, Greece and its significance for the Cycladic Massif. *Geologische Rundschau*, **72**, 283–299.

VAN HINSBERGEN, D. J. J. 2004. *The evolving anatomy of a collapsing orogen*. PhD Thesis, University Utrecht, The Netherlands. *Geologica Ultraiectina*, **243**, 1–280.

VAN HINSBERGEN, D. J. J., SNEL, E., GARSTMAN, S. A., MARUNTEANU, M., LANGEREIS, C. G., WORTEL, M. J. R. & MEULENKAMP, J. E. 2004. Vertical motions in the Aegean volcanic arc: evidence for rapid subsidence preceding volcanic activity on Milos and Aegina. *Marine Geology*, **209**, 329–345.

VAN HINSBERGEN, D. J. J., HAFKENSCHEID, E., SPAKMAN, W., MEULENKAMP, J. E. & WORTEL, M. J. R. 2005*a*. Nappe stacking resulting from subduction of oceanic and continental lithosphere below Greece. *Geology*, **33**, 325–328.

VAN HINSBERGEN, D. J. J., LANGEREIS, C. G. & MEULENKAMP, J. E. 2005*b*. Revision of the timing, magnitude and distribution of Neogene rotations in the western Aegean region. *Tectonophysics*, **396**, 1–34.

VANDENBERG, L. C. & LISTER, G. S. 1996. Structural analysis of basement tectonites from the Aegean metamorphic core complex of Ios, Cyclades, Greece. *Journal of Structural Geology*, **18**, 1437–1454.

VANDERHAEGHE, O. 2004. Structural development of the Naxos migmatite dome. *In*: WHITNEY, D. L., TEYSSIER, C. & SIDDOWAY, C. S. (eds) *Gneiss Domes in Orogeny*. Geological Society of America Special Paper, **380**, 211–227.

VANDERHAEGHE, O. & TEYSSIER, C. 2001. Crustal-scale rheological transitions during late-orogenic collapse. *Tectonophysics*, **335**, 211–228.

VIGNER, A. 2002. *Images sismiques par réflexions verticales et grand-angle de la croûte en contexte extensif: les Cyclades et le fossé Nord-Egéen*. PhD Thesis, Institut de Physique du Globe de Paris, University Paris 7.

WALCOTT, C. R. & WHITE, S. H. 1998. Constraints on the kinematics of post-orogenic extension imposed by stretching lineations in the Aegean region. *Tectonophysics*, **298**, 155–175.

WDOWINSKI, S. & AXEN, G. J. 1992. Isostatic rebound due to tectonic denudation: a viscous flow model of a layered lithosphere. *Tectonics*, **11**, 303–315.

WEGMANN, M. I. 2006. *Die Entwicklung des Rb/Sr-Isotopensystems in metamorphen Mikrostrukturen in Abhängigkeit von Temperatur, Druck und Mineralkomposition am Beispiel der Hochdruckmetamorphite von Südevia, Griechenland*. Fachbereich Geowissenschaften, Freie University, Berlin, Germany.

WERNICKE, B. 1992. Cenozoic extensional tectonics of the U.S. Cordillera. *In*: BURCHFIELD, B. C., LIPMAN, P. W. & ZOBACK, M. L. (eds) *The Cordilleran Orogen: Conterminous U.S., The Geology of North America*. Geological Society of America, **43**, 553–581.

WIJBRANS, J. R. & MCDOUGALL, I. 1988. Metamorphic evolution of the Attic Cycladic Metamorphic Belt on Naxos (Cyclades, Greece) utilizing $^{40}Ar/^{39}Ar$ age spectrum measurements. *Journal of Metamorphic Geology*, **6**, 571–594.

WIJBRANS, J. R., SCHLIESTEDT, M. & YORK, D. 1990. Single grain argon laser probe dating of phengites from the blueschist to greenschist transition of Sifnos (Cyclades, Greece). *Contributions to Mineralogy and Petrology*, **104**, 582–593.

WIJBRANS, J. R., VAN WEES, J. D., STEPHENSON, R. A. & CLOETINGH, S. A. P. L. 1993. Pressure- temperature-time evolution of the high-pressure metamorphic complex of Sifnos, Greece. *Geology*, **21**, 443–446.

WIJNS, C., WEINBERG, R., GESSNER, K. & MORESI, L. 2005. Mode of crustal extension determined by rheological layering. *Earth and Planetary Science Letters*, **236**, 120–134.

WUST, S. L. 1986. Regional correlation of extension directions in Cordilleran metamorphic core complexes. *Geology*, **14**, 828–830.

ZEILINGA DE BOER, J. 1989. The Greek enigma: is development of the Aegean orogene dominated by forces related to subduction or obduction? *Marine Geology*, **87**, 31–54.